JGR Oceans

RESEARCH ARTICLE
10.1029/2023JC019937

Interannual Variability of Subpolar Mode Water in the Subpolar North Atlantic

I. Stendardo[1], B. Buongiorno Nardelli[2], S. Durante[2,3], D. Iudicone[4], and D. Kieke[1,5]

[1]University of Bremen, Institute of Environmental Physics, Bremen, Germany, [2]Istituto di Scienze Marine, Consiglio Nazionale delle Ricerche, Rome, Italy, [3]Istituto per lo studio degli impatti Antropici e Sostenibilità in ambiente marino, Consiglio Nazionale delle Ricerche, Rome, Italy, [4]Stazione Zoologica Anton Dohrn di Napoli, Naples, Italy, [5]Bundesamt für Seeschifffahrt und Hydrographie (BSH), Hamburg, Germany

Key Points:

- Subduction of water below the mixed layer is driven by entrainment with advection modulating the small-scale dynamics
- Volume and formation of Subpolar Mode Water changes every year in size and location
- The difference between the formation rate from the thermodynamic and kinematic approaches suggests a large role of diapycnal mixing

Supporting Information:

Supporting Information may be found in the online version of this article.

Correspondence to:

I. Stendardo,
ilaria.stendardo@uni-bremen.de

Citation:

Stendardo, I., Buongiorno Nardelli, B., Durante, S., Iudicone, D., & Kieke, D. (2024). Interannual variability of Subpolar Mode Water in the Subpolar North Atlantic. *Journal of Geophysical Research: Oceans*, *129*, e2023JC019937. https://doi.org/10.1029/2023JC019937

Received 17 APR 2023
Accepted 4 MAR 2024

Author Contributions:

Conceptualization: I. Stendardo, B. Buongiorno Nardelli, D. Iudicone, D. Kieke
Data curation: B. Buongiorno Nardelli
Formal analysis: I. Stendardo, B. Buongiorno Nardelli, S. Durante
Funding acquisition: I. Stendardo, B. Buongiorno Nardelli
Investigation: I. Stendardo
Methodology: I. Stendardo, B. Buongiorno Nardelli, S. Durante, D. Iudicone
Project administration: I. Stendardo
Visualization: I. Stendardo
Writing – original draft: I. Stendardo

Abstract Subpolar Mode Water (SPMW) is an important water mass originating in the eastern North Atlantic. Its formation, subject to modification through oceanic interior mixing, can directly influence the volume of water contributing to the Atlantic meridional overturning circulation. Utilizing observation-based data sets spanning from 1993 to 2018, we estimated the formation rates and volume of SPMW within isopycnal layers and examined its temporal variability. Two complementary approaches were used to estimate the formation rate: a thermodynamic approach focusing on the air-sea interactions and a kinematic approach involving volume transport from the mixed layer to the ocean's interior, including the entrainment/detrainment of the mixed layer itself. This is the first time that thermodynamic and kinematic approaches are applied to observation-based data in the North Atlantic. Our results suggest a substantial role of diapycnal mixing in diluting the dense waters formed by air-sea fluxes toward the range of SPMW densities. The study reveals a complex interplay of processes, with entrainment being the primary driver of subduction/obduction rates, while advection contributes to the overall small-scale dynamics. Variations in the volume and location of SPMW formation are observed from year to year. Notably, when SPMW forms extensively in lighter isopycnal layers, the volume occupied by denser isopycnals decreases and vice versa. We attributed this compensation effect to a propagation signal, where formation in the lightest isopycnal bins influences the formation in denser isopycnal bins with a delay of a few years, emphasizing the circulation's role in shaping the SPMW distribution.

Plain Language Summary We present an analysis of one important type of water mass, the Subpolar Mode Water (SPMW) located in the North Atlantic Ocean. We looked at data collected over a period of 26 years from 1993 to 2018, to understand how SPMW forms and how its volume changes over time. We used two different methods to calculate how much SPMW forms each year to have the best possible picture. One method looked at air-water interactions, and the other at how the water moves from the top layer of the ocean to deeper parts. This is the first time these methods are applied to observation-based data in the North Atlantic. Our findings highlight the important role of water mixing in changing the density of SPMW. We also found that one of the main reasons how the SPMW leaves the top layer of the ocean is through the shoaling/deepening of the mixed layer itself over time, modulated horizontally by the small-scale dynamics of the ocean. Additionally, the volume of SPMW and location where it forms can vary from year to year. Notably, when SPMW forms in larger amounts in the upper part of the ocean, there is less SPMW in the denser water.

1. Introduction

Subpolar Mode Water (SPMW) is a large volume of water in the upper 1,000 m of the water column of the subpolar North Atlantic (Brambilla & Talley, 2008). It originates in the eastern and northeastern subpolar North Atlantic and represents a variety of near-surface waters of intermediate densities, occupying the layers between the ocean surface and the permanent pycnocline (e.g., Brambilla et al., 2008). It is characterized by a thick layer of nearly uniform properties like temperature, salinity, oxygen and density (e.g., McCartney & Talley, 1982). SPMW is found along the pathways of the several branches of the North Atlantic Current (NAC, see the general circulation scheme in Figure 1a). Following the cyclonic pathway of the upper ocean circulation in the subpolar gyre, SPMW density increases downstream (Brambilla & Talley, 2008; Petit et al., 2021). Part of this water mass is advected toward the Irminger Sea, the Labrador Sea and the Nordic Seas where it contributes to the formation of the North Atlantic Deep Water (NADW) (de Boisséson et al., 2012; Petit et al., 2021).

Writing – review & editing: I. Stendardo, B. Buongiorno Nardelli, S. Durante, D. Iudicone, D. Kieke

NADW forms the cold and deep limb of the Atlantic meridional overturning circulation (AMOC) (Buckley & Marshall, 2016; Jackson et al., 2022; Zhang et al., 2019), which in turn affects global climate. For this reason, SPMW has received increasing scientific attention over the past years (de Boisséson et al., 2012; Petit et al., 2021). Knowledge on SPMW formation and transformation has been gained by analyzing in situ observations (e.g., Brambilla & Talley, 2008; Brambilla et al., 2008; Petit et al., 2021) and numerical ocean models (e.g., Marsh et al., 2005), at times combining them with chlorofluorocarbon data (Trossman et al., 2012), as well as Lagrangian modeling (e.g., de Boisséson et al., 2012). All these studies agree that SPMW is formed during winter when the mixed layer depths reach their maxima. Although these maxima are not comparable to those observed during winter deep convection in the Labrador Sea, SPMW can be considered the pre-conditioned water mass from which NADW is formed. This occurs through further densification downstream in the Irminger and Labrador Seas (Petit et al., 2021). SPMW plays a relevant role in taking up carbon, oxygen, heat and other properties from the atmosphere and transporting them down to the ocean interior (Iudicone et al., 2011; Li et al., 2021).

Brambilla et al. (2008) and Brambilla and Talley (2008) described the average properties of SPMW, its mean circulation, its origin and transformation based on historical hydrographic data. They showed that SPMW formed during late winter convection does not follow the cyclonic circulation of the subpolar gyre while gradually increasing its density due to buoyancy loss, as originally suggested by McCartney and Talley (1982). Instead, they associated a different SPMW with each of the several north-eastward branches of the NAC, which are not necessarily connected by a cyclonic flow. SPMWs associated with each NAC branch are continuously densified downstream (Brambilla & Talley, 2008) by diapycnal fluxes. However, isopycnal fluxes contribute significantly to the SPMW throughput, alongside the dominant diapycnal volume fluxes. Brambilla et al. (2008) suggest that the isopycnal contribution could range from 10% to 40% of the diapycnal flux. Thus, a certain SPMW characterized by a specific density can be considered as the source of a denser SPMW within the same current branch (Brambilla et al., 2008).

A few studies looked at interannual and long-term variability of SPMW (de Boisséson et al., 2012; Stendardo et al., 2015). More recently, Petit et al. (2021) analyzed about 40 years of observations (1980–2019, with a focus on the 2014–2019 period), to identify the role of air-sea fluxes and ocean surface density in the production of SPMW. Buoyancy flux and surface area of the source waters in the density range between $\sigma_\theta = 27.3$–27.5 kg m^{-3} were correlated with SPMW transformation in the Iceland Basin. They showed that SPMW formation and transformation is mainly influenced by the density changes of the ocean surface. Locally, the surface density is determined by a combination of horizontal advection, wind-driven upwelling and air-sea fluxes. According to Petit et al. (2021), the air-sea fluxes could explain only about 30% of changes in the wintertime surface density field. It is thus striking that other mechanisms, such as diapycnal mixing, horizontal and vertical advection, are needed to account for the remaining 70% of observed change.

Petit et al. (2021) especially highlighted the winter of 2014–2015. This winter was characterized by an unusually large SPMW transformation in terms of surface area and intensity observed in the Iceland Basin. They associated the largest SPMW transformation in 40 years with the combination of a strong buoyancy forcing and a large source area. Grist et al. (2016) showed an exceptionally strong heat loss in the winter of 2013–2014, causing a strong formation of SPMW. Through a trajectory study, they established that this anomalously cold SPMW formed in the winter of 2013–2014 re-emerged in the mixed layer in the following winter of 2014–2015 (about 77% of the water formed in the previous winter), which could explain the large formation of SPMW observed in Petit et al. (2021).

Finally, these extreme winter conditions in 2014–2015 seem to be responsible for the rapid cooling and freshening of the upper ocean in the following years until 2017, when the minimum in temperature (Desbruyères et al., 2019) and salinity was reached (Biló et al., 2022; Fox et al., 2022; Holliday et al., 2020). Desbruyères et al. (2019) predicted that this rapid cooling of the upper ocean in the eastern North Atlantic, mainly occupied by SPMW in the eastern part, would be feeding an intensification of the AMOC with 5-year delay. This would be occurring through increased light-to-dense water transformations. Due to atmospheric forcing, this would eventually lead to extreme warming of the subpolar gyre at least until 2021. Recent studies show that after the minimum in temperature observed in 2017, the subpolar gyre is now heading toward a warmer and more saline state as predicted by Desbruyères et al. (2019) and confirmed by Desbruyères et al. (2021) and Biló et al. (2022).

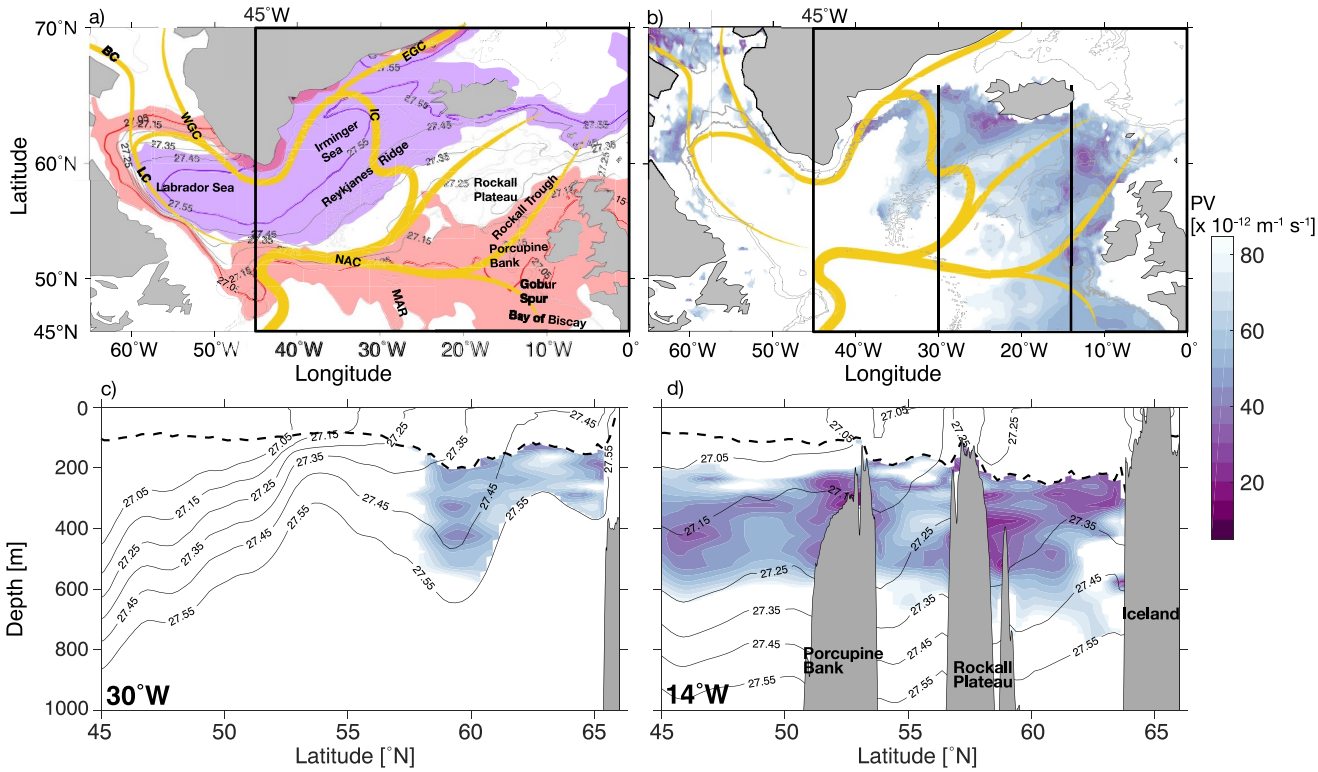

Figure 1. (a) Upper ocean circulation schematic (yellow) highlighting the pathways of the North Atlantic Current (NAC), the Irminger Current (IC), the East Greenland Current (EGC), the West Greenland Current (WGC), the Baffin Island Current (BC) and the Labrador Current (LC) in the subpolar gyre. Gray contours denote the location of the isopycnals $\sigma_\theta = 27.05$–27.55 kg m^{-3} (every 0.1 kg m^{-3}) outcropping in winter (DJFM), averaged from 1993 to 2018. The red contour represents the mean location of the upper bound ($\sigma_\theta = 27.05$ kg m^{-3}) of the chosen SPMW density range, the red shade is the spatial range of this isopycnal during 1993–2018. Similarly, the purple contour represents the deeper bound ($\sigma_\theta = 27.55$ kg m^{-3}) of the chosen SPMW density range and the respective spatial range over the years of interest. The regional focus of this study is highlighted by the black rectangle. (b) Spatial horizontal distribution of SPMW represented here as a mean of potential vorticity (PV [10^{-12} m^{-1} s^{-1}]) from 1993 to 2018 in the density range $\sigma_\theta = 27.05$–27.55 kg m^{-3}. Only those values with PV below 80×10^{-12} m^{-1} s^{-1} and located below the mixed layer are displayed. Vertical black lines denote the two locations of the two sections displayed in (c) at 30°W and in (d) at 14°W showing the vertical distribution of PV and density. The dashed lines in (c) and (d) represent the mean mixed layer depth. All estimates were obtained from the ARMOR3D data set. Bathymetry at 1,000 and 2,000 m is also displayed with gray contour lines from ETOPO2.

Some of the above-mentioned studies (Brambilla & Talley, 2008; Brambilla et al., 2008; Desbruyères et al., 2019; Grist et al., 2016; Petit et al., 2021) made use of the possibility to estimate the water mass formation (in this specific case SPMW formation) through air-sea interaction by using only surface buoyancy fluxes and sea surface density data (Speer & Tziperman, 1992). This approach is named *thermodynamic approach* and has been often applied in the North Atlantic Ocean (Marsh et al., 2005; Marshall et al., 1999; Speer & Tziperman, 1992) to quantify the transformation and formation rates associated with air-sea interactions. Surface water mass transformation driven by air-sea fluxes, however, only tells us part of the story as, on one hand, ventilated water masses can be further modified by mixing in the interior of the ocean, and, on the other hand, anomalies in the volume of SPMW can directly modulate the amount of water feeding the overturning circulation. This leads to the necessity to also assess the direct transfer of water at the base of the mixed layer toward the interior of the ocean, a process named subduction. The Eulerian approach to determine the subduction rate is called *kinematic approach*. It involves estimating the contribution of the 3D transport across the mixed layer base and the entrainment/detrainment of the mixed layer itself. Previous studies (Marsh et al., 2005; Petit et al., 2021) have examined the interannual variability of water mass formation, with one study utilizing a model and the other relying on observations. However, none of these studies incorporates both thermodynamic and kinematic approaches simultaneously.

Our study aims to analyze the formation of SPMW in the eastern North Atlantic over the past three decades (1993–2018). Here, we take advantage of two 3D gridded hydrographic and velocity products, namely ARMOR3D (Guinehut et al., 2012; Mulet et al., 2012) and OMEGA3D (Buongiorno Nardelli, 2020a), both from

the Copernicus Marine Service. The data sets are combined with a reanalysis data set for the air-sea fluxes, ERA5 (Dee et al., 2011) from the European Center for Medium-Range Weather Forecasts (ECMWF). We utilize these observation-based data to describe the rates and changes in the formation process of SPMW and investigate their potential impact on the local volume and distribution of SPMW. When discussing "formation" in our study, we refer to both the formation resulting from the divergence of diapycnal fluxes caused by air-sea interaction (thermodynamic approach) and the volume transport of water from the mixed layer to the ocean's interior through subduction (kinematic approach). We thus aim at extending previous analyses. These either focused only on the mean state of the SPMW (Brambilla et al., 2008; Brambilla & Talley, 2008) and were based on a limited amount of data from the winter season, or limited to specific regions and periods (de Boisséson et al., 2012; Stendardo et al., 2015). While others considered only the thermodynamic estimates (e.g., Petit et al., 2021).

2. Data and Methods

2.1. Data Sets

To analyze the spatial and temporal variability of the SPMW's volume, we use a multi-observation global ocean 3D data set (ARMOR3D, 2021) that is distributed by the Copernicus Marine Service (Guinehut et al., 2012; Mulet et al., 2012). ARMOR3D covers the period from 1993 to the present. The period chosen in this study is 1993–2018, which is the time range in common with the other data sets used for this analysis and presented in this section.

ARMOR3D provides hydrographic properties like temperature, salinity, geostrophic velocities and mixed layer depth. We use delayed time mode (DT) data on a global regular grid resolved at ¼°. The vertical range is from the surface down to a depth of 5,500 m. The data set incorporates 50 vertical levels with finer resolution in the upper 1,500 m of the water column (between 5 and 100 m) and coarser resolution below (between 250 and 500 m). For our study, we use the weekly resolution, which represents a weekly value centered on Wednesdays.

ARMOR3D is a combination of in situ observations and satellite data processed in three steps. Details on the data processing can be found in Guinehut et al. (2012). Major steps involve statistical regressions to retrieve synthetic T/S fields from the surface down to 1,500 m. These fields are combined in a second step with the available in situ profiles for T and S using an optimal interpolation algorithm. The outcome of this second processing step is the ARMOR3D combined fields for the upper 1,500 m of the water column. In the final step, the 3D fields are expanded to the water column below 1,500 m incorporating T/S fields from seasonal World Ocean Atlas 2018 (WOA18) climatology. The advantage of ARMOR3D over other gridded data sets that simply interpolate in situ profiles (e.g., EN4) lies in this multi-step combination of in situ observations and satellite data that in our opinion allows to significantly increase the accuracy and effective resolution of the reconstructed fields. According to the Quality Information Document from the Copernicus Marine Service (ARMOR3D, 2021) temperature at 10 m has a root mean square (RMS) error from 0.6°C to 1.1°C, where the lower value corresponds to the best RMS over the Argo period (2003–2018), whereas the upper value corresponds to RMS over the pre-Argo period (1993–2003). At 100 m the RMS goes from 0.8°C to 1.4°C and at 1,000 m from 0.2°C to 0.5°C. Salinity RMS at 10 m goes from 0.1 to 0.2, at 100 m from 0.1 to 0.15 and at 1,000 m from 0.02 to 0.07. Regarding the geostrophic currents, the Quality Information Document (ARMOR3D, 2021) explains that the velocities are slightly too barotropic with a bias in the zonal component on the period from 1998 to 2017 of around 0.0006 m s^{-1} and in the meridional component close to zero. The RMS differences are around 0.064 m s^{-1} for the zonal component and 0.052 m s^{-1} for the meridional component. Finally, the mixed layer depth (MLD) has an RMS of 29 m.

For the calculation of the water mass formation using the kinematic approach, we consider an observation-based data set of 3D ocean currents. This product, named OMEGA3D (Buongiorno Nardelli, 2020b), is based on the application of a quasi-geostrophic diagnostic model to ARMOR3D data and is also distributed by the Copernicus Marine Service. It covers the period from 1993 to 2018 and provides 3D fields of vertical and horizontal currents estimated through a diagnostic model based on a diabatic version of the Omega equation (Buongiorno Nardelli, 2020a; Giordani et al., 2006):

$$\nabla_h \cdot \left(N^2 \nabla_h \cdot w\right) + f^2 \frac{\partial^2 w}{\partial z^2} = \nabla_h \cdot Q \tag{1}$$

where w is the vertical velocity, N^2 is the Brunt-Väisälä frequency, f is the Coriolis parameter, h denotes the horizontal components and Q is the forcing associated with different processes: kinematic deformation, turbulent buoyancy and turbulent momentum. Buongiorno Nardelli et al. (2018) and Buongiorno Nardelli (2020a) provide an extensive introduction to the method and the equations used to retrieve the horizontal and vertical currents. OMEGA3D is available on the same regular global grid and has the same time resolution as ARMOR3D. On the vertical scale, it differs from ARMOR3D since it has a finer resolution from the surface down to 1,500 m (75 depth levels).

This product has been extensively validated before its release through the Copernicus Marine Service (Buongiorno Nardelli, 2020b), as also detailed in Buongiorno Nardelli (2020a). The global RMS differences for the horizontal components attain approximately around 0.10 m s^{-1} at 15 and 0.06 m s^{-1} at 1,000 m depth with distinct geographical variations. Larger discrepancies are expected in the equatorial zone and coastal areas making the product only suited for open ocean application (Buongiorno Nardelli, 2020a). Given their relatively small magnitude, vertical velocities cannot be measured in the open ocean (order of 1–100 m d^{-1}). Consequently, the validation of the vertical velocity in OMEGA3D faces limitations due to the absence of direct observational benchmarks. The validation of OMEGA3D was thus obtained by indirect assessment of the divergent components of the quasi-geostrophic horizontal currents and by intercomparison with available model re-analysis data. Buongiorno Nardelli (2020a) compared the vertical velocities with the output of two ocean climate reanalysis systems that contain vertical velocity time series of comparable length (SODAv3.4.2 and ECCOv4r4). The large-scale patterns and range of values found in the averaged velocities are quite similar among the three products, though OMEGA3D shows higher variance, mostly driven by mesoscale signals that are not resolved in lower resolution products such as ECCOv4r4. Maximum absolute mean values reach around 2 m d^{-1}. Areas dominated by large-scale, wind-driven upwelling at high latitudes and by downwelling at mid-latitudes are consistently identified in the three products, with values rarely exceeding 0.5 m d^{-1}.

For the calculation of the water mass formation using the thermodynamic approach, we use the ECMWF Reanalysis v5 (ERA5) data set (Hersbach et al., 2023) provided by the Copernicus Climate Change Service (C3S). ERA5 is the fifth generation of the ECMWF reanalysis for the global climate and weather and covers the periods from 1959 to the present. We use the gridded product with ¼° resolution on single levels from 1993 to 2018. We further use hourly data and average them as daily values regarding the evaporation and precipitation rates and all components that are necessary to calculate the total heat fluxes.

2.2. Identification of SPMW and Volume Calculation

The high vertical homogeneity of SPMW manifests itself through low values of an approximated estimate of the potential vorticity (PV) (only including the effect of stratification). PV can be used as a proxy to identify SPMW in the isopycnal layers (Brambilla & Talley, 2008). We calculated PV following Brambilla and Talley (2008) as:

$$PV = \left| \frac{f}{\rho} \frac{\delta \rho}{\delta z} \right| \tag{2}$$

where f is the Coriolis parameter, and ρ is the density referenced to the midpoint of the depth interval z. Using a similar criterion as in Brambilla and Talley (2008), we identify SPMW as water that has a PV lower than 80×10^{-12} m^{-1} s^{-1}. However, different from their work, we consider only the amount of SPMW below the mixed layer depth since we are interested in the part of SPMW that potentially leaves the mixed layer and might eventually contributes to the deep water formation. This minimum in PV is found in the density range $\sigma_\theta = 27.05$–27.55 kg m^{-3}, in the upper 1,000 m of the water column (Figures 1c and 1d). Before calculating PV, we interpolated all the ARMOR3D profiles on a vertical grid of 5 m.

The choice of a specific PV minimum value to identify SPMW is rather arbitrary. For example, Brambilla and Talley (2008) used PV values between 40 and 100 $\times$ 10^{-12} m^{-1} s^{-1} found in the density range σ_θ = 27.3–27.5 kg m^{-3}. Petit et al. (2021) used a PV value below 40×10^{-12} m^{-1} s^{-1} for the identification of SPMW across the Iceland Basin that occupies the same density range σ_θ = 27.3–27.5 kg m^{-3}. The choice of the upper bound σ_θ = 27.05 kg m^{-3} in our study serves to include into our analysis the formation and transformation of lighter variety of SPMW near the Porcupine Bank and Bay of Biscay in the eastern North Atlantic. These regions also show low PV below 80×10^{-12} m^{-1} s^{-1} (Figure 1). Brambilla et al. (2008) analyzed the density range $\sigma_\theta = 27.05$–

27.95 kg m^{-3}, defining as SPMW the density range between $\sigma_\theta = 27.3$–27.5 kg m^{-3}. We chose $\sigma_\theta = 27.55$ kg m^{-3} as the deeper SPMW bound to exclude intrusions of Labrador Sea Water (LSW; Kieke et al., 2007) and Irminger Sea Intermediate Water (ISIW; Le Bras et al., 2020). Both represent rather fresh and relatively denser water masses formed by winter deep convection in the Labrador Sea and Irminger Sea and are also characterized by low PV values (e.g., Le Bras et al., 2020; McCartney & Talley, 1982).

In order to calculate the volume of SPMW we considered five isopycnal bins of 0.1 kg m^{-3} width. From the weekly data, we added up the thickness of SPMW at each grid point within each isopycnal bin below the MLD having a PV lower than 80×10^{-12} m^{-1} s^{-1}. The volume estimates obtained from the weekly data are then averaged as monthly and annual mean values. SPMW formation occurs in the winter season when certain isopycnals outcrop at the surface. Therefore, we have computed the annual mean over the period ranging from December of the previous year to November of the follow-up year to better catch the formation period of this water mass. As a result, the year 1993 is the average of only 11 months, while all other years completely cover 12 months.

Figure 1 illustrates the spatial distribution of SPMW in the subpolar North Atlantic, both vertically and horizontally. Notably, some shallow waters exhibiting properties similar to SPMW are observed in the Baffin Bay and in the Labrador Sea. However, these regions are not included in our volume calculations, which focus solely on the SPMW formation region east of 45°W (black rectangle in Figures 1a and 1b). The presence of SPMW is clearly observed along the eastern rim of the subpolar North Atlantic, extending from the Bay of Biscay to the Irminger Sea. Vertical sections (Figures 1c and 1d) reveal the thickness of SPMW, reaching up to 800 m. These sections also highlight the south-to-north shoaling of the density field within the SPMW layer. Winter outcrop areas indicate the regions where the SPMW forms (Figure 1a), with denser types of SPMW forming along the rims of the Irminger Sea ($\sigma_\theta > 27.45$ kg m^{-3}) in the northern regions of the Northeast Atlantic and lighter types forming in the Iceland Basin and Rockall Trough and Porcupine Bank regions.

2.3. SPMW Formation

Changes in the amount of SPMW that is formed during winter can in part be expected to modulate the variability of SPMW volume below the mixed layer locally, but also to feed and drive the variability of the SPMW transport away from its formation areas.

Most of the thermodynamical forcing involved in the transformation of these water masses is provided by the interaction with the atmosphere. Cooling/heating and precipitation/evaporation, induce changes in temperature and salinity and transform surface waters from one density to another (Speer & Tziperman, 1992). In fact, as the surface water transformation rates are not constant across the affected density ranges, water can be removed from some density ranges and accumulate at others (Walin, 1982). The major part of the upper layer of the eastern subpolar North Atlantic, namely between the ocean surface and the permanent pycnocline, is dominated by the presence of SPMW (Brambilla & Talley, 2008). Thus, determining the formation rate of this water mass through buoyancy fluxes and corresponding density changes is a useful heuristic approach, despite it neglects the impact of mixing.

The transfer of fluid from the base of the mixed layer into the interior thermocline, known as subduction, plays a crucial role in communicating surface water-mass properties to the ocean's interior (Marshall, 1997). In an ideal ocean without diffusive processes, the thermodynamic and kinematic approaches are closely linked. The subduction of a fluid between two density surfaces, integrated across the ocean from coast to coast, would match the formation driven by air-sea fluxes in a steady state (Iudicone, Madec, et al., 2008; Marshall et al., 1999). However, the real ocean deviates from this ideal scenario due to the presence of diffusive processes. Consequently, estimating water mass formation requires considering both the surface transformation driven by air-sea interactions and the subduction processes. These estimates provide essential complementary information. The former is an integral assessment of the rate of creation and destruction of water masses solely due to air-sea interactions, while the latter quantifies the exchange of fluid between the mixed layer and the stratified interior below (Marshall et al., 1999). Several studies have applied the kinematic approach to determine the subduction rate of specific water masses (e.g., Courtois et al., 2020; Da Costa et al., 2005; Kwon et al., 2013; Qiu & Huang, 1995). However, none of these studies specifically focused on the SPMW, and only a limited number of studies have compared the two approaches, mainly in the context of thermocline water

masses of the Southern Ocean (Karstensen & Quadfasel, 2002) and numerical model results for the North Atlantic (Marshall et al., 1999).

2.3.1. Kinematic Approach

With the kinematic approach, we calculated the rate at which a water parcel crosses the mixed layer base toward the ocean's interior (Marshall et al., 1999). This combines the vertical and horizontal velocities from the OMEGA3D data set along with associated estimates of MLD. To determine the net subduction rates (Sr) as defined in Equation 3, we integrated the vertical and horizontal volume fluxes across the instantaneous mixed layer base over a complete annual cycle using weekly OMEGA3D velocities. Additionally, we accounted for changes in the mixed layer volume by addressing variations of the MLD over time, which is referred to as "entrainment/detrainment" (Figure 2a).

$$Sr = \frac{\partial h}{\partial t} + \vec{u}_h \cdot \nabla h + w_h \tag{3}$$

where h is the mixed layer depth, and $\vec{u}_h$ and w_h are the velocity components at the base of the mixed layer.

The resulting positive rates are the subduction rates, while the negatives are the obduction rates. It is important to stress that no "perfect" assessment of subduction/obduction rates can be based on Eulerian approaches, as true water mass transformation evaluation would imply tracking the fate of individual water parcel along Lagrangian trajectories. Other operational definitions of net subduction have been thus adopted in the literature (see also Kwon et al., 2013; Marshall, 1997) often limiting to the fluxes across a time-invariant winter maximum mixed layer (e.g., Buongiorno Nardelli et al., 2018). In those cases, only the exchange rate to the main pycnocline is considered. Significant differences can be expected with respect to the instantaneous approach followed here, most likely due to diapycnal processes that occur within the seasonal pycnocline (Kwon et al., 2013; Nishikawa et al., 2010).

Since OMEGA3D has a different vertical resolution than ARMOR3D, the MLD used for the kinematic approach needs to be re-estimated. We estimate the instantaneous MLD as the depth at which a density difference of 0.03 kg m^{-3} is found with respect to the density at the surface (see also Buongiorno Nardelli et al., 2017; de Boyer Montégut et al., 2004). Then, we compute the volumetric flow rate across the mixed layer base by estimating separately the contribution of the horizontal, vertical and entrainment terms, respectively. Instantaneous values are then integrated between December of the previous year and November of the follow-up year to analyze the interannual variations in the spatial patterns and intensity of the subduction rates. The yearly mean net subduction/obduction rates focus on predefined density bins to identify and track specific water mass changes. Specifically, as for the volume calculation, we have divided the density range into five isopycnal bins of 0.1 kg m^{-3} width, covering the density range between $\sigma_\theta = 27.05$ and 27.55 kg m^{-3}. Using yearly net subduction estimates we aim at quantifying the amount of water that is transferred from the upper boundary layer to the interior ocean over one complete destratification/stratification annual cycle (Stommel, 1979).

2.3.2. Thermodynamic Approach

The transfer of water into the thermocline must be supported by the formation of surface water through heat and freshwater fluxes (Karstensen & Quadfasel, 2002; Marshall et al., 1999). With the thermodynamic approach, this transformation is estimated using the buoyancy fluxes calculated from ERA5. The convergence/divergence of this transformation flux yields to creation/destruction of water masses by air-sea fluxes (Marshall et al., 1999). To quantify the transformation rates, we calculated first the buoyancy fluxes (kg m^{-2} s^{-1}) from the heat and freshwater fluxes as follows:

$$bf = -\alpha \frac{Q_{tot}}{c_p} + \beta (E - P) S \tag{4}$$

where the coefficient of thermal expansion of seawater (α in $°C^{-1}$), the haline contraction coefficient (β), the heat capacity of seawater (c_p in J kg^{-1} $°C^{-1}$) and surface salinity (S) are derived from ARMOR3D data. The surface net heat flux (Q_{tot} in W m^{-2}) and the net freshwater fluxes, expressed as evaporation minus precipitation (E-P in

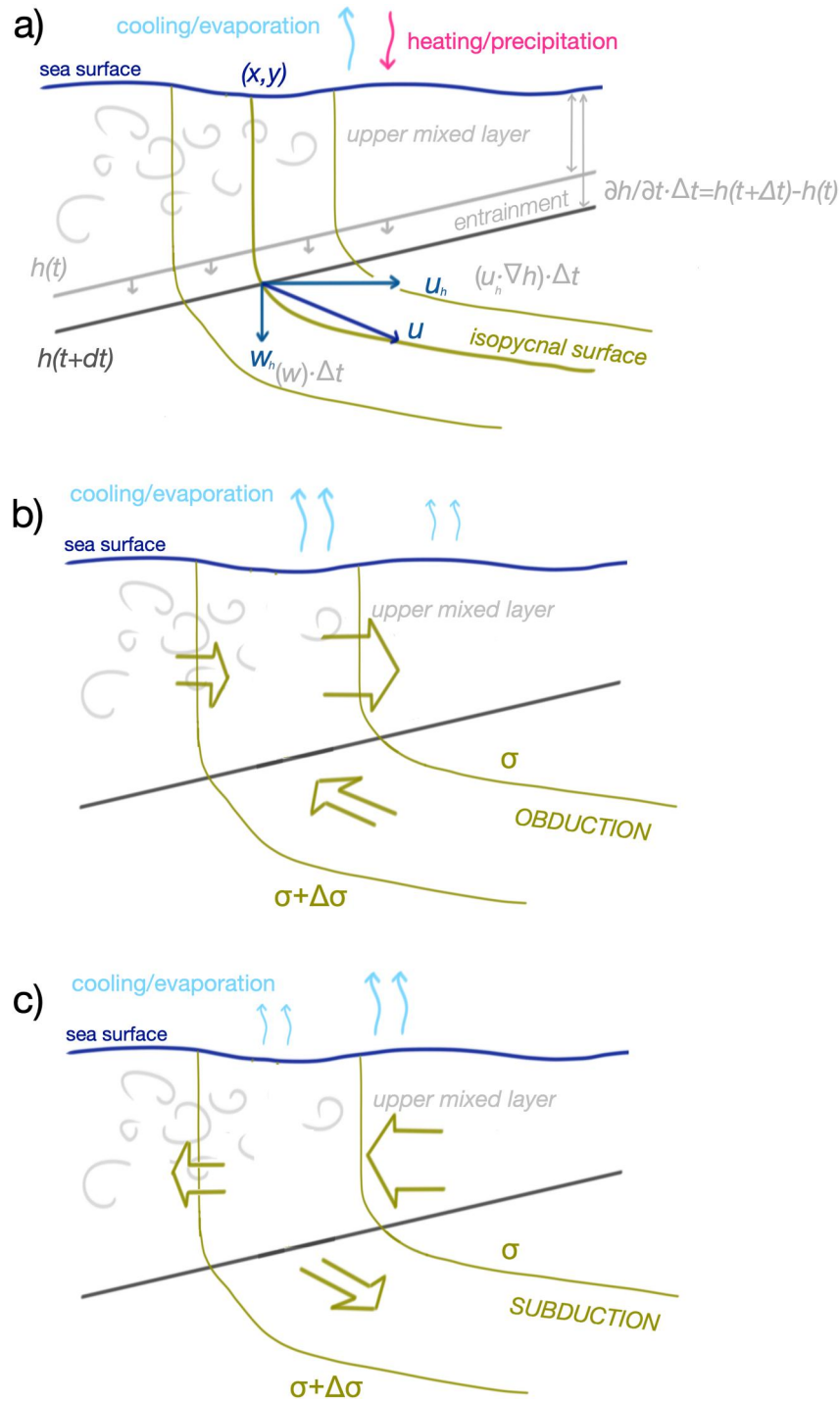

Figure 2. (a) Subduction rate in a Eulerian frame of reference where a water parcel at the base of the mixed layer moves with velocity of $(\vec{u}_h, w_h)$ while the mixed layer base itself deepens from the light gray line to the black line. (b) negative formation rate (net obduction) from the ocean interior to the mixed layer driven by the divergence of surface water mass transformation (based on Marshall et al., 1999; see also Brambilla et al., 2008; Groeskamp et al., 2019; Iudicone, Madec, & McDougall, 2008) (c) positive formation rate (net subduction) from the surface mixed layer to the ocean interior driven by the convergence of surface water mass transformation (based on Brambilla et al., 2008).

kg m^{-2} s), are calculated from ERA5 reanalysis data. The hourly data from ERA5 are averaged daily. To make the surface fluxes sampling consistent with ARMOR3D and OMEGA3D which both have one value per week centered on Wednesdays, we selected one value per week centered on Wednesdays also in ERA5. However, we also made all the calculations with the daily values in order to compare the results with previous studies (Brambilla et al., 2008; Marsh et al., 2005; Speer & Tziperman, 1992). Following Speer and Tziperman (1992) the annual transformation rates (F_{σ_θ} in Sv) integrated over the area bound by the outcropping isopycnals σ_θ^1 and σ_θ^2 is calculated as follows (Marsh et al., 2005):

$$F_{\sigma_\theta} = \frac{1}{t}\sum_{n=1}^{t}\frac{1}{\Delta\sigma_\theta}\sum_{i,j}\left[\Delta A_{i,j}\, bf_{i,j}\, \Pi\left(\sigma_\theta^1 - \sigma_\theta^2\right)\right] \quad (5)$$

where σ_θ is the potential density at which the transformation rate is calculated. It is worth mentioning that this "classical" formulation of water mass transformation does not take into consideration the penetrative solar shortwave radiation in the estimation of surface buoyancy fluxes. This term can have a significant impact especially in the tropical, subtropical and upwelling regions (Iudicone, Madec, & McDougall, 2008). We computed the transformation for the isopycnal range from σ_θ = 26–27.6 kg m^{-3} binned by 0.1 kg m^{-3} ($\Delta\sigma_\theta$) for each grid point i,j. The chosen isopycnal range allows to compare our results with other studies that look at the water mass transformation for the entire North Atlantic, and not specifically for the SPMW (e.g., Speer & Tziperman, 1992). t is the time, which in this case represents the number of weeks for each year from 1993 to 2018, A is the area of each grid point within the isopycnal bin, $\Pi\left(\sigma_\theta^1 - \sigma_\theta^2\right)$ is a sampling function, which takes the value 1 if $\sigma_\theta^2 \le \sigma_{\theta,surf} \le \sigma_\theta^1$, otherwise the value is 0 (Marsh et al., 2005). From the annual mean transformation, we calculate the annual mean formation as follows (Brambilla et al., 2008; Groeskamp et al., 2019; Speer & Tziperman, 1992):

$$M_{\sigma_\theta} = F_{\sigma_\theta^2} - F_{\sigma_\theta^1} \quad (6)$$

where $\sigma_\theta^2 < \sigma_\theta < \sigma_\theta^1$. M_{σ_θ} represents the annual mean volume flux that accumulates (or is removed) between the isopycnal σ_θ^2 and σ_θ^1, which should be comparable with (but not equal to) the annual net subduction rate calculated with the kinematic approach referred to the same isopycnal bin (Iudicone, Madec, et al., 2008). As explained by Iudicone, Madec, et al. (2008), the subduction rate is a purely kinematic concept that gives us a measure of the total transport from the mixed layer into the interior, partially compensated during the year by the transport in the opposite direction into the mixed layer, the so-called obduction (Iudicone, Madec, et al., 2008). As illustrated by for example, Marshall et al. (1999) and Groeskamp et al. (2019), the two values may diverge due to diffusive fluxes at the base of the mixed layer and across isopycnals in the mixed layer. Thus, if we consider that the net annual formation rate estimated using the thermodynamic approach is partially compensated by transport into the mixed layer, an important relationship emerges. Specifically, the formation rate can be expressed as the difference between the annual subduction rate and the annual obduction rate per isopycnal layer. This relationship can be represented as: surface dianeutral fluxes + diffusive dianeutral fluxes = subduction − obduction. That means, it is plausible to have a huge subduction rate even if the net water-mass formation (surface dianeutral fluxes + diffusive dianeutral fluxes) adds up to zero (Iudicone, Madec, et al., 2008). Diffusive transfer of buoyancy within the mixed layer comes from vertical mixing, which is significant everywhere in the upper boundary layer of the ocean. This explains the differences arising from the kinematic and thermodynamic methods (Marshall et al., 1999). Moreover, Marshall et al. (1999) show that at high latitudes, lateral fluxes provide an additional significant transfer of buoyancy.

There is also another component that should be considered when comparing the formation rates derived by the two approaches. Marshall et al. (1999) described that in absence of diffusive processes, the subduction of fluid between a certain isopycnal bin is comparable with the formation driven by air-sea fluxes. This similarity occurs when the fluid is integrated across the ocean from one coast to the other, essentially crossing closed boundaries. In absence of closed boundaries, as in our study region (rectangle box in Figures 1a and 1b), the differences between the subduction from the kinematic approach and the formation rate from the thermodynamic approach are thus also caused by the lateral volume flux across the open boundaries within the mixed layer (Nishikawa et al., 2013). This lateral flux can be calculated as follows:

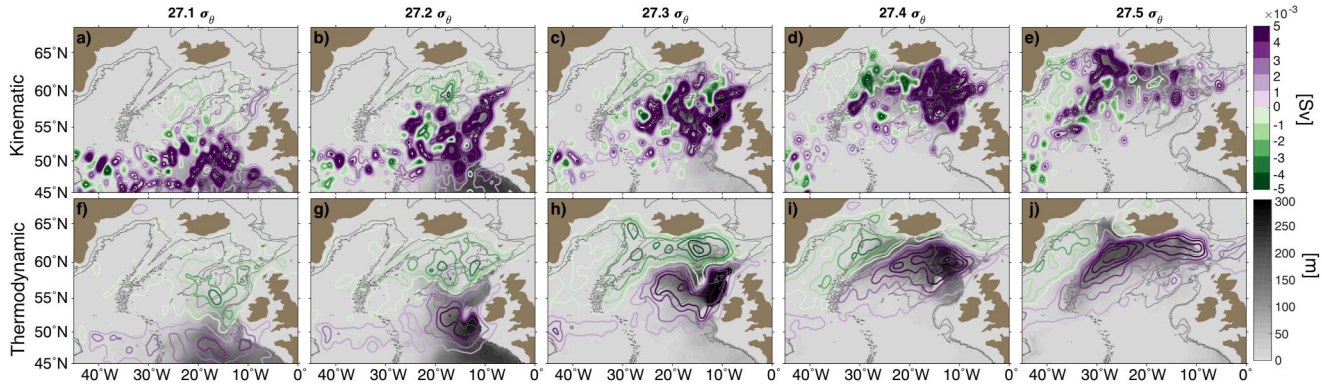

Figure 3. Mean state of the SPMW layer thickness [m] (1993–2018) represented as filled contours with a gray color scheme for the isopycnal bins centered at $\sigma_\theta = 27.1$ kg m^{-3} (a and f), $\sigma_\theta = 27.2$ kg m^{-3} (b and g), $\sigma_\theta = 27.3$ kg m^{-3} (c and h), $\sigma_\theta = 27.4$ kg m^{-3} (d and i) and $\sigma_\theta = 27.5$ kg m^{-3} (e and j). Superimposed with purple/green contour lines is the mean formation rate [Sv] for the same time period calculated with the kinematic approach (a–e) and with the thermodynamic approach (f–j). The purple contour lines denote positive values and the green contour lines negative values. Bathymetry at 1,000 and 2,000 m is also displayed with gray contour lines and taken from ETOPO2.

$$I = \oiint \vec{u} \cdot \hat{n}\, dA \tag{7}$$

Where $\vec{u}$ is the geostrophic currents from ARMOR3D in the zonal and meridional direction and $\hat{n}$ is the normal unit vector of the boundaries (outward negative), and A is the area along the lateral boundaries within the mixed layer at each isopycnal bin. We calculated the instantaneous lateral volume flux across the four boundaries of each isopycnal bin above the MLD and then calculated the net flux in or out of the box to assess the lateral advection within the mixed layer.

Following Brambilla et al. (2008) we also calculated the spatial distribution of the annual mean transformation and formation rate in addition to the space and time integral. Its annual distribution will be displayed as maps.

3. Results and Discussion

3.1. SPMW Mean State

As expected, we found most of the SPMW below the mixed layer between $\sigma_\theta = 27.05$ and 27.55 kg m^{-3} in the eastern basin of the North Atlantic and along the boundary of the Irminger Sea between Iceland and Greenland (Figures 1b and 3). This is in agreement to some extent with the distribution of SPMW described by Brambilla and Talley (2008), although we found that SPMW in the density bin centered at $\sigma_\theta = 27.3$ kg m^{-3} is more spread toward the center of the eastern basin (Figures 3c and 3h) rather than closer to the boundaries. Also the isopycnal bins centered at $\sigma_\theta = 27.4$ and 27.5 kg m^{-3} (Figures 3d and 3i; 3e and 3j) are not only limited to the boundaries, as shown in Brambilla and Talley (2008), but have a larger spread toward the center of the eastern North Atlantic. Differences are of course expected due to the different criteria used to identify SPMW and to the different data sets used. Brambilla and Talley (2008) identified SPMW in the isopycnal at 27.3 kg m^{-3} with a PV below 100×10^{-12} m^{-1} s^{-1} regardless of whether it is above or below the mixed layer depth. Based on this criterion, we would have expected a wider extension of the SPMW, but differences can be expected also for other reasons, such as the use of different data sets that covers different time periods. Brambilla and Talley (2008) used hydrographic bottle data collected from 1900 to 1990 and WOCE hydrographic cruises (the latest one considered in 2003), which contain only few winter data. Our data set is restricted to the satellite altimeter era (1993–2018) and it has a year-round coverage.

The spatial distribution of SPMW within a particular isopycnal layer, identified by its thickness, exhibits a notable agreement with its formation rate calculated from both approaches (Figure 3). However, the formation rate derived from the kinematic approach displays higher noise due to the influence of mesoscale features. Interestingly, a portion of the water formed in each isopycnal layer is transported back into the mixed layer in the northern section of the formation area, as indicated by negative formation values in Figure 3 (green contour lines).

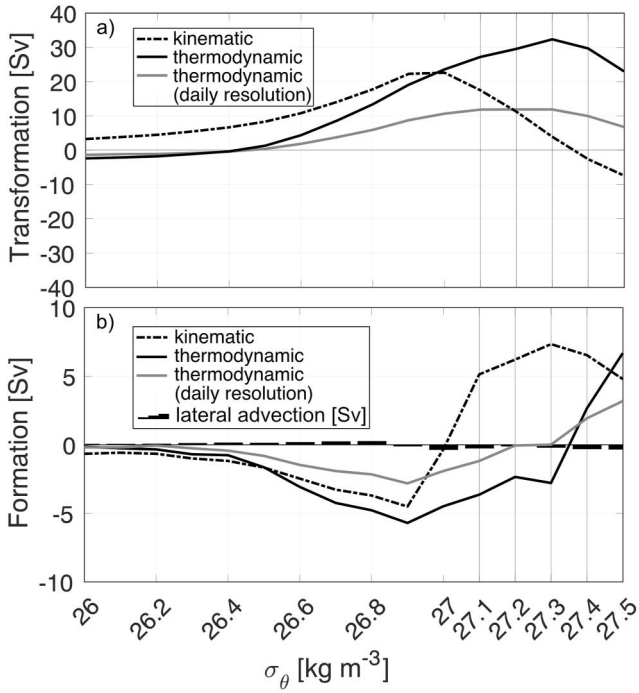

Figure 4. Transformation rate (a) and formation rate (b) over the period from 1994 to 2018 in the isopycnal bins from $\sigma_\theta = 26$ kg m^{-3} to 27.5 kg m^{-3} within the study region. Black line shows the thermodynamic estimates and dot-dashed lines the kinematic ones. The gray lines are the thermodynamic estimates using the daily buoyancy values derived from ERA5. The black bars in panel (b) denote the lateral advection within the mixed layer [Sv] in the study area (outward negative). Vertical lines highlight the SPMW domain.

The two different methods agree on the main patterns. Thus, positive formation driven by the convergence of surface water mass transformation from a thermodynamic point of view (Figures 3f–3j) corresponds mostly to a net subduction from the surface mixed layer into the ocean interior from a kinematic point of view (Figures 3a–3e). Vice versa, a negative formation (Figures 3f–3j) driven by the divergence of surface water mass transformation corresponds mostly to a net obduction (Figures 3a–3e) from the ocean interior toward the mixed layer. However, the kinematic approach shows markedly higher values than the thermodynamic approach and, as already mentioned, larger noise. This results in a less homogenous separation between regions of positive formation and regions of negative formation.

In contrast to the classical hypothesis proposed by McCartney and Talley (1982), which suggests the direct transformation of an entire density of SPMW into the next denser SPMW, Brambilla et al. (2008) proposed that the transformation of SPMW occurs separately within each NAC branch. This hypothesis was based on their observations of a negative formation rate for the isopycnal bin at $\sigma_\theta = 27.3$ kg m^{-3} in the southern part of the subpolar gyre, opposed to a positive formation rate in the northern part. These findings indicated a relatively strong divergence aligning with the north-eastward flow of one of the NAC branches. The authors proposed that water from the ocean interior upwells into the mixed layer, replenishing the loss of this specific isopycnal. However, our results do not support this analysis. Neither the kinematic nor the thermodynamic approach revealed positive formation and subduction in the southern part of the subpolar gyre, and negative values in the northern part for the same isopycnal bin. Therefore, our findings confirm the classical hypothesis put forth by McCartney and Talley (1982).

To get a clearer picture of the ongoing processes, it is useful to look at the mean water transformation and formation rates over a wider density range (Figures 4a and 4b). The thermodynamic estimates show that air-sea interactions sustain an increasing transformation rate between $\sigma_\theta = 26$ to 27.3 kg m^{-3}, corresponding to water mass consumption (negative value, Figure 4b), with the core of the (positive) water mass formation occurring in the range between $\sigma_\theta = 27.4$ and 27.5 kg m^{-3}. This is in agreement with Grist et al. (2016) and Brambilla et al. (2008), who used a similar approach to calculate water mass transformation and formation using buoyancy fluxes. Instead, in Marsh et al. (2005) the core of water mass formation occurs between $\sigma_\theta = 27.2$ and 27.8 kg m^{-3} when using a thermodynamic approach applied to model outputs. Transformation rates calculated using the kinematic approach, however, show that formation takes place already at $\sigma_\theta = 27$ kg m^{-3}, increasing until $\sigma_\theta = 27.3$ kg m^{-3} and with declining rates in the denser ranges. This apparent discrepancy calls for a substantial role of diapycnal mixing in diluting the denser waters sustained by air-sea fluxes toward the range of SPMW densities, as suggested by Marshall et al. (1999). This hypothesis is strengthened by the fact that the lateral fluxes across the open boundaries of our domain play a negligible role. Their values are of an order of magnitude smaller than the formation rate (Figure 4b). This confirms that SPMW primarily forms through air-sea fluxes and mixing with minimal contribution from lateral advection within the mixed layer. Nishikawa et al. (2013) showed that the lateral advection of a specific current from the north (Oyashio Current) significantly influences the formation of denser Central Mode Water (CMW) in the Pacific Ocean near Japan. However, for lighter CMW and Subtropical Mode Water (STMW), lateral advection seems irrelevant. The formation of water in these cases is primarily attributed to air-sea fluxes in the STMW and the diapycnal mixing in the lighter CMW (Nishikawa et al., 2013).

Another study from Portela et al. (2020) shows that subduction and diapycnal mixing in the Subantarctic Mode Water (SAMW) in the Southern Ocean accounts for most of the volume trend within this water mass. Similar to the SPMW, SAMW is found at intermediate depths between 500 and 1,000 m, thus far from the surface and the bottom where diapycnal mixing is most important (Cerovečki et al., 2013; Portela et al., 2020; Rintoul, 2018). Portela et al. (2020) hypothesized that the role of diapycnal mixing in the SAMW comes from the proximity of this water mass to the MLD, where wind forcing, mesoscale eddies and downward propagation of internal waves enhance diapycnal mixing (Rintoul, 2018; Sloyan et al., 2010). Considering that SAMW and SPMW form in a

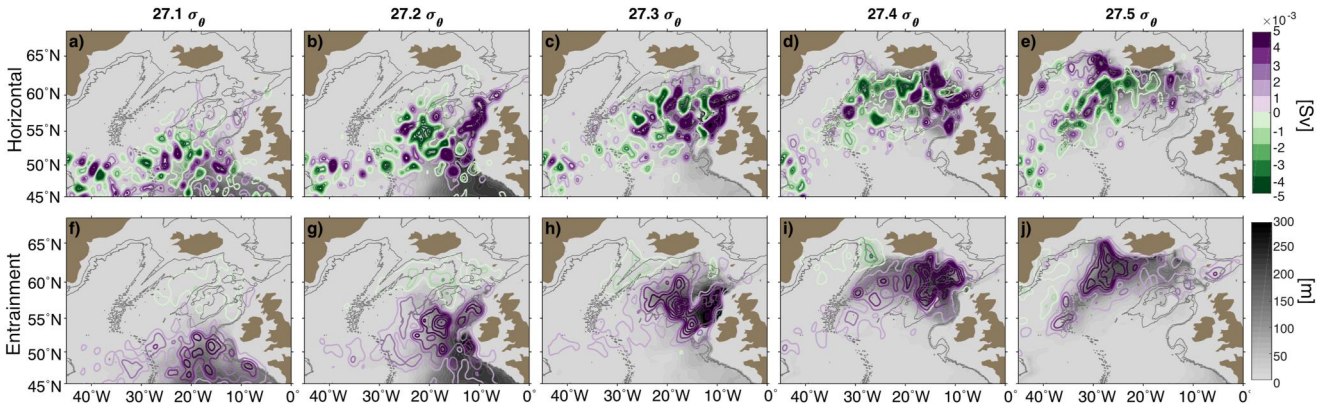

Figure 5. Mean state of the SPMW layer thickness [m] (1993–2018) same as Figure 3. Superimposed with purple/green contour lines is the mean state of the horizontal component [Sv] (a–e) and the entrainment component [Sv] (f–j) of the subduction/obduction rate from the kinematic approach. The purple contour lines denote positive values and the green contour lines negative values. Bathymetry at 1,000 and 2,000 m is also displayed with gray contour lines.

similar way, it is plausible to consider that this hypothesis can also be applied to the SPMW in the North Atlantic. Another study based on a high-resolution model (Xu et al., 2018) mapped the diapycnal water mass transformation in the upper North Atlantic Ocean and also agrees that surface buoyancy loss does not account for all the transformation. Mixing is responsible for significant transformation around the subpolar gyre (Xu et al., 2018), especially along the steep isopycnal slopes. A more recent study in the North Atlantic (Fröhle et al., 2022), based on a Lagrangian analysis on an eddy-rich ocean model, highlights the substantial role of water mass formation below the sea surface due to diapycnal mixing.

We need to point out here that in order to be able to compare directly the results of the thermodynamic approach with the one from the kinematic approach all the data sets need to have the same time resolution. As we described in the method session, OMEGA3D has a sample per week centered on Wednesday. Thus, although the atmospheric data from ERA5 are on hourly resolution allowing us to actually calculate daily fluxes, we calculated the buoyancy fluxes using one sample per week to be consistent with the OMEGA3D and ARMOR3D data sets. However, when the thermodynamic calculation is done using daily data, the resulting transformation and formation estimates (Figure 4) are lower than the one calculated from the mean weekly fluxes, and they are closer to the ones calculated by for example, Grist et al. (2016) and Brambilla et al. (2008). Moreover, the formation at $\sigma_\theta = 27.3$ kg m^{-3} is close to zero when using the daily fluxes and not negative as obtained from the weekly averaged data (Figure 4b).

The kinematic approach allows for a separate analysis of the individual components contributing to the net transport across the mixed layer, which in turn determines the subduction and obduction rates. These components are derived from both the vertical and horizontal velocities, as well as the temporal variations in the MLD. Particularly, the entrainment component, which is influenced by the shoaling or deepening of the mixed layer itself, is not directly dependent on the velocity of water mass across the mixed layer base. Consequently, when there is a rapid deepening of the MLD, water that has previously left the mixed layer has the potential to re-enter it. Conversely, a swift shoaling of the MLD allows water to escape from the mixed layer and move toward the interior of the ocean. Kwon et al. (2013) suggested this as the primary mechanism driving the subduction of mode waters in the Southern Ocean. They argued that the detrainment of mixed layer waters into the stratified pycnocline occurs during early spring over an expanded outcrop area. A similar hypothesis was also drawn by Brambilla et al. (2008) for the SPMW in the North Atlantic. In Figure 5, we compared the horizontal and entrainment components. We did not include a map of the vertical component because our computations showed that it has a negligible contribution over the entire domain (one to two orders of magnitude smaller than the other two terms). This is supported by the small vertical component needed to allow motion along a sloping isopycnal surface. Similarly to Kwon et al. (2013), we found that the entrainment component is the main mechanism driving the subduction/obduction rates (Figures 5f–5j), with the horizontal component mostly acting as a modulator (Figures 5a–5e). In the two companion papers from Brambilla et al. (2008) and Brambilla and Talley (2008) it was argued that the net formation of SPMW obtained from the thermodynamic approach can be interpreted as the loss by the entrainment to the interior layers due to vigorous mixing that strongly alters the SPMW properties. This is

in agreement with our results. However, Brambilla et al. (2008) excluded completely that the formation of SPMW results from the classical advection of water from the mixed layer down along the isopycnals since they did not detect any PV minimum below the base of the winter mixed layer (Brambilla & Talley, 2008). With the kinematic approach we do observe a prevailing contribution of the entrainment versus the other components, however, the advective contribution does also play a role and cannot be ruled completely out. Moreover, we do observe SPMW below the winter mixed layer although of course its volume is smaller than the one during the summer period (not shown).

When comparing the two components with the formation rates from the thermodynamic approach (Figures 3f–3j), the pattern of the entrainment (Figures 5f–5j) seems to agree better with the thermodynamic approach than the horizontal component (Figures 5a–5e). The latter is clearly modulated by variability of 3D transport at the mesoscale, showing much less uniform patterns and also displaying obduction in regions where both the entrainment and the thermodynamic approach would indicate subduction. According to Petit et al. (2021), variance in the air-sea fluxes can explain alone about 30% of changes in the wintertime outcrop area over the Iceland Basin. It should not be too surprising that the entrainment compares better with the formation rate calculated using the air-sea fluxes with the thermodynamic approach since shoaling and deepening of the MLD are linked to air-sea fluxes.

3.2. Temporal Changes of SPMW Formation Rates and Volume

Thanks to the observation-based data sets used in this study we are not only able to compare the formation rates obtained from the two different approaches from a "climatological" point of view but we are also able to compare their changes on interannual time scales. In the following, we present and discuss the temporal changes of formation and volume of the SPMW in each isopycnal bin in the period 1993–2018.

During these 26 years, the depths of the isopycnals show large fluctuations (Figure 6). The maximum depth change might reach up to several hundred meters: noteworthy are the periods between 1994 and 1998, between 2013 and 2015, and between 2015 and 2018 for the densest isopycnals. The shoaling/deepening of the isopycnals is associated with changes in PV. Higher PV values occur when the isopycnal layers of SPMW are located deeper (indicating reduced exchanges of water at the base of the mixed layer), such as in 1998 and 2013. Lower values show up when the SPMW layers are shallower (increased exchange of water at the base of the mixed layer), such as in 1994 and 2015 (Figure 6).

During these same periods, the winter MLD also exhibited significant variability, with anomalies reaching up to 400 m. This variability consistently shows that when the isopycnals deepen and PV increases, the MLD becomes shallower. Conversely, when the isopycnals become shallower and PV decreases, the MLD deepens (Figure 6). The shoaling and deepening of isopycnals within the water column directly influence changes in the outcrop area. During shoaling of the isopycnals, the outcrop area expands, whereas during deepening, it contracts (Figure 7). When the isopycnals shoal, denser isopycnal come directly into contact with the surface ocean or with the base of the mixed layer, resulting in the formation of new mode waters. The correlation between the changes of the outcrop area and the rate of shoaling/deepening of the MLD explains the variability of the net volume subduction of mode waters out of the mixed layer in the Southern Ocean (Kwon et al., 2013). But also, more recent studies (Petit et al., 2021) focusing on the SPMW formation in the North Atlantic highlight how, for example, the winter 2014–2015 was characterized by a relatively large outcrop area of the isopycnals between σ_θ = 27.3 and 27.5 kg m^{-3} that covers most of the Iceland Basin, which results in a large formation of SPMW. Our findings (Figure 7) indicate a strong correlation between extensive outcrop areas and deeper mixed layers, and vice versa. Furthermore, deeper mixed layers tend to exhibit higher salinity and temperature within the isopycnal bins that surface. Although this may appear counterintuitive, as deeper MLD would typically be associated with colder and fresher water columns, it is important to consider that deeper mixed layers occur within wider outcrop areas in regions with significant horizontal gradients in salinity and temperature. Some exceptions are observed, however, for example, at the isopycnal bins σ_θ = 27.4 and 27.5 kg m^{-3} during 2002, when a deepening of the mixed layer is associated with a small outcrop area and consequently lower salinity and temperature. Furthermore, with respect to the prominent signal observed in 2015 within the densest isopycnal bin at σ_θ = 27.5 kg m^{-3}: the presence of a similar signal in the lightest isopycnal bin at σ_θ = 27.1 kg m^{-3} as early as 2013, and in the intermediate bins (σ_θ = 27.2 and 27.3 kg m^{-3}) in 2014, suggests a gradual propagation of the signal from lighter to denser isopycnal bins. However, there is a lag of few years is this propagation. This spreading phenomenon is also evident when the

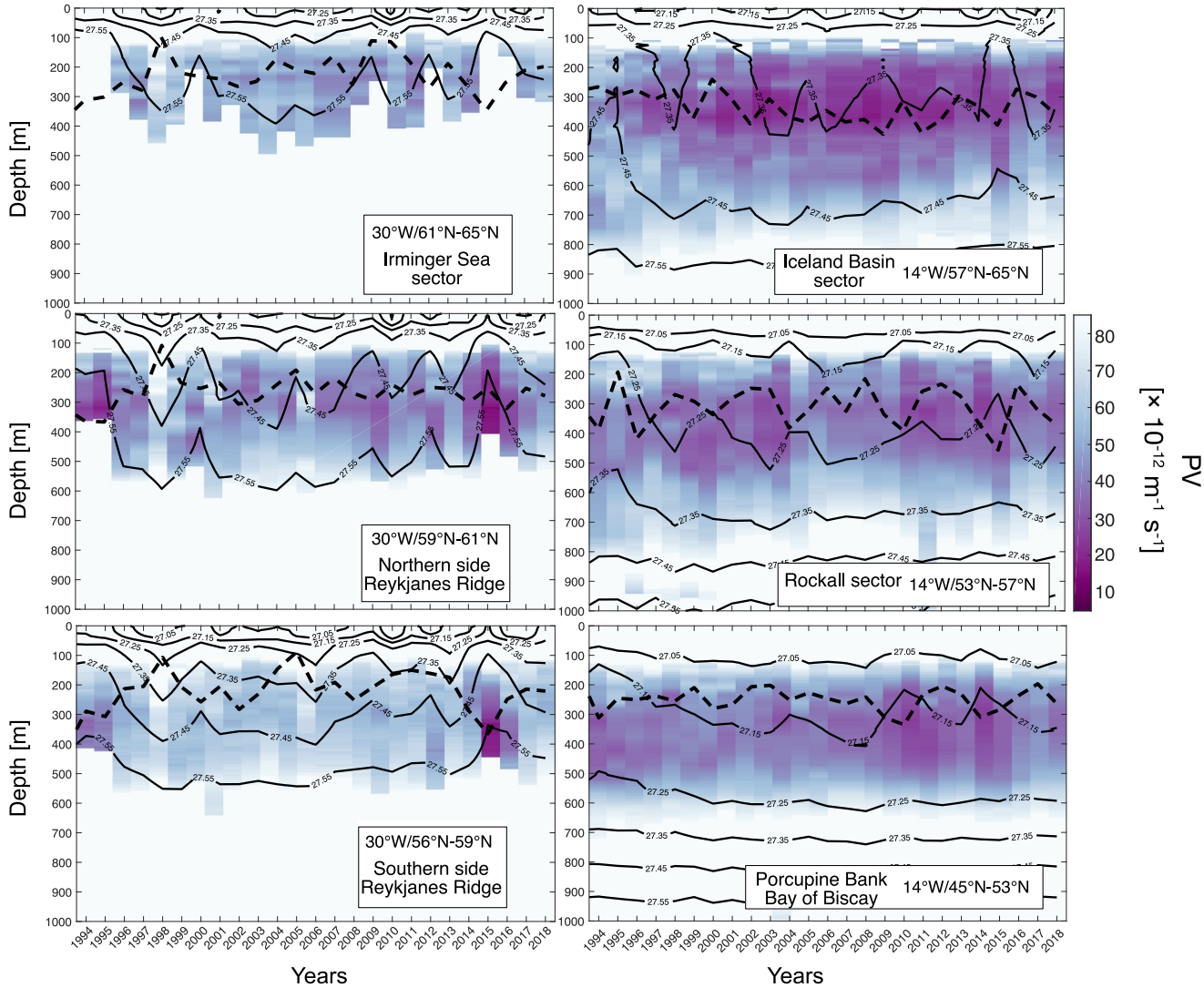

Figure 6. Hovmöller diagrams showing the temporal changes of potential vorticity [$\times 10^{-12}$ m^{-1} s^{-1}] (filled colors), potential density σ_θ [kg m^{-3}] (black contour lines) and winter mixed layer depth (JFM, black dashed lines) from 1994 to 2018 in the water column. The left panels show the temporal variability from 0 to 1,000 m along the section at 30°W divided into three subsections: 61°N–65°N, 59°N–61°N, and 56°N–59°N. The right panels show the temporal variability from 0 to 1,000 m along the section at 14°W divided into three subsections: 57°N–65°N, 53°N–57°N, and 45°N–53°N.

surface outcrop area reaches its minimum, as observed in 1998 within the isopycnal bin at $\sigma_\theta = 27.5$ kg m^{-3}. In this case, a corresponding minimum in the outcrop area was observed in 1995 within the isopycnal bin at $\sigma_\theta = 27.1$ kg m^{-3}.

Periods characterized by significant shoaling of the MLD, accompanied by reduced outcrop areas of the deeper isopycnal layers (Figures 7a and 7b), such as in 1998, 2004, 2010, 2013 and 2017 (green bars in Figure 7), align with periods a weakened subpolar gyre and a westward retraction of its front, as shown by the subpolar gyre index proposed by Berx and Payne (2017). Their gyre index is defined as the first principal component of an empirical orthogonal function analysis of the sea level anomaly field in the North Atlantic Ocean. Conversely, instances of MLD deepening followed by increased outcrop areas in deeper isopycnal layers, such as in 1995, 2000, 2009, 2015 and 2018 (purples bars in Figures 7a and 7b), correspond to periods with positive values of the gyre index, signifying a wider spread of the subpolar front (Berx & Payne, 2017).

The eastern subpolar North Atlantic experienced a large freshening between 2012 – 2016, as reported by Holliday et al. (2020). This freshening was attributed to an unusual winter wind pattern that influenced the ocean circulation, including a slowdown of the NAC, resulting in a reduced input of subtropical water into the eastern North

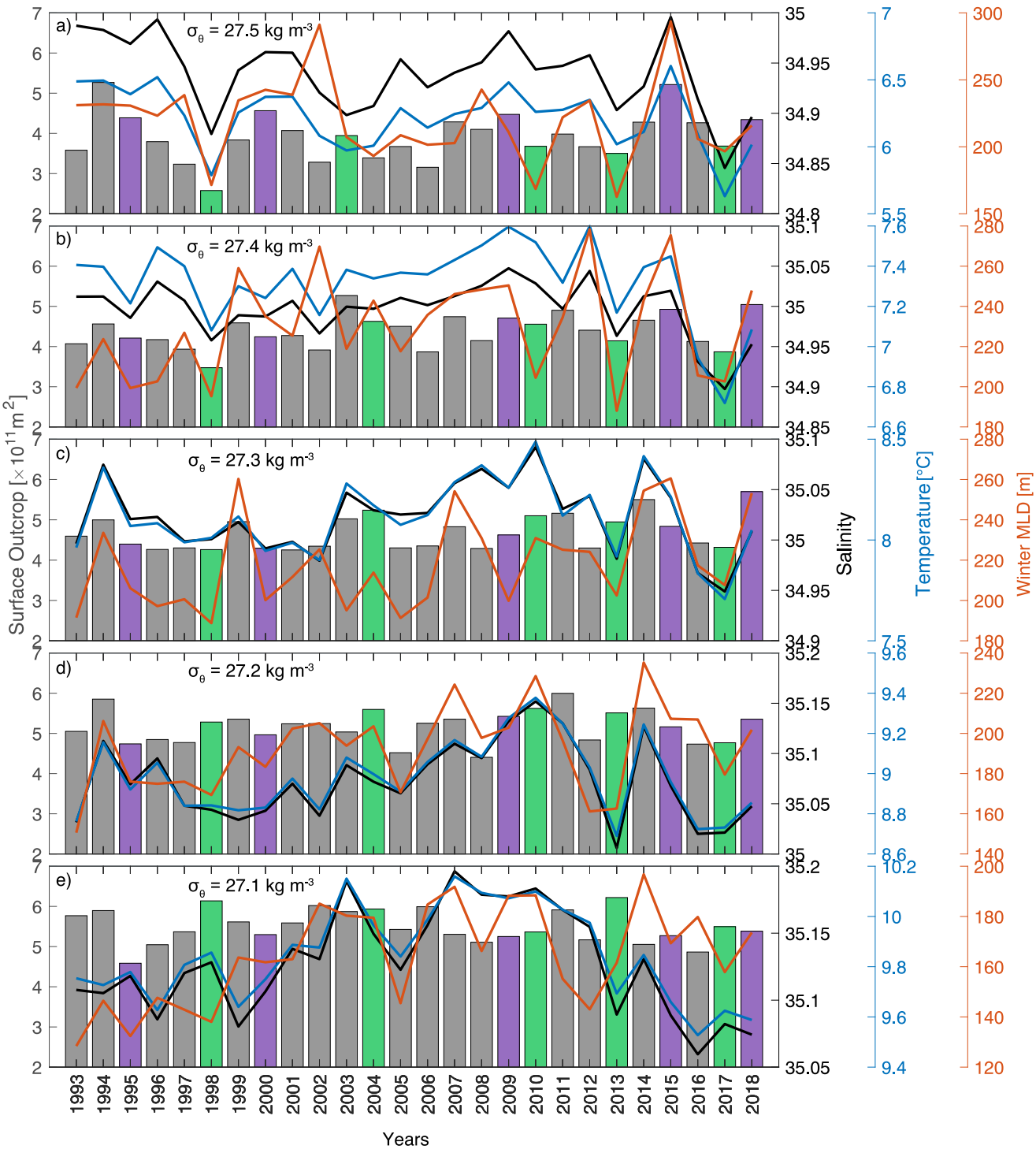

Figure 7. Annual mean of the surface outcrop areas [$\times 10^{11}$ m^2] represented by the gray bars for each isopycnal bin from (a) $\sigma_\theta = 27.5$ kg m^{-3} to (e) $\sigma_\theta = 27.1$ kg m^{-3}, compared to the respective temperatures [°C] (blue lines), salinity (black lines) and winter (JFM) MLDs [m] (orange lines) within the outcrop area at the time when the isopycnals outcrop at the surface. Purple and green bars highlight the years used to calculate the composites 1 and 2 shown in Figure 9.

Atlantic. Consequently, there was an increased propagation of freshwater from the western boundary into the eastern basin. In a more recent study, Biló et al. (2022) referred to this freshening as the "new great salinity anomaly" (GSA), which arrived in the Irminger Sea between 2015 and 2020. This GSA contributed to the suppression of the deep convection in the Irminger Sea in the subsequent winters after 2018. Biló et al. (2022)

noted that the GSA primarily affected the SPMW layers, which eroded and reduced in size over time. The decrease in SPMW formation was attributed to a reduced inflow of subtropical water, which prevented its transformation into SPMW by air-sea fluxes. Consistent with these recent finding (Biló et al., 2022; Holliday et al., 2020), our results indicate an initial increase in surface salinity and temperature that continued until 2010 in the southern part of the subpolar gyre, specifically within the lightest density bins ranging from $\sigma_\theta = 27.1$ to 27.2 kg m^{-3} (Figures 7c–7e). This was followed by a rapid cooling and freshening until 2016. While it may be surprising not to observe a similar trend in the densest isopycnal layers (Figures 7a and 7b), even with a certain delay, moving toward the core of the subpolar gyre introduces greater complexity in the gyre's dynamic. Previous studies (Fox et al., 2022; Fratantoni & McCartney, 2010; Standardo et al., 2020) have shown that the gyre's dynamic is influenced not only by the advection of warm and saline subtropical water along the pathway of the NAC but also by the advection of fresh and cold subpolar water from the western boundary regions toward the east. The strong high salinity and temperature observed in 2015 within the densest isopycnal bins (Figures 7a and 7b) may be a result of the increased salinity and temperature observed in the lightest isopycnal bins in 2014 (Figures 7e and 7d). Fox et al. (2022) attributed the freshening and cooling after the 2016 to the advection of Labrador Current in the eastern North Atlantic rather than to a decrease in the northward transport of warmer and saline surface subtropical water. This advection led to significant freshening in the subpolar gyre until at least 2017. As suggested by Biló et al. (2022), SPMW formation starts to strengthen after 2015, which is consistent with our results.

The formation rates of SPMW exhibit significant variability throughout the entire period, as indicated by both the kinematic and the thermodynamic estimates (Figures 8a and 8b). When examining the two time-series in Figures 8a and 8b, substantial differences in formation rates can be expected between the two approaches, as water masses can form also below the surface ocean due to diapycnal mixing (Fröhle et al., 2022). In our study, there is a substantial disparity between the thermodynamic and kinematic approaches regarding where net subduction starts to occur within the isopycnal layers. According to the thermodynamic approach, net subduction primarily occurs on the densest isopycnal bins, beginning at 27.4 kg m^{-3} (see Figure 4b). Yearly formation rates (Figure 8b) reveal that net subduction can also occur at lighter isopycnals, such as in 1998 and 2010. These are also the years highlighted in green in Figure 7 when lighter isopycnals occupy a larger area at the surface at the expense of the denser isopycnals, which occupy a smaller area. On the other hand, in other years like 1994, 1995 and 2015 net subduction only occurs at the isopycnal at 27.5 kg m^{-3} (Figure 8b), which occupies the largest surface area (Figure 7). In contrast, the kinematic approach generally suggests that net subduction begins already at the isopycnal bin 27.1 kg m^{-3} (refer to Figure 4b). Here as well, the yearly mean formation rate exhibits some interesting variability compared to the general mean (Figure 8a). For instance, in 1994, 1995, and 2015 net subduction only occurs until reaches the isopycnal at 27.4 kg m^{-3}, while the densest isopycnal indicates a net obduction. This obduction appears to be driven in these cases by the horizontal component (Figure 8d). These are the years that also demonstrate such large formation due to air-sea fluxes, implying that during those years, the denser SPMW formed due to air-sea fluxes is diluted and consumed due to mixing. These results are in agreement with Marsh et al. (2005), who found a negative mixing-driven formation rate indicating consumption of water mass within the region of formation. A study from Fröhle et al. (2022), also highlights the substantial role of diapycnal mixing in the export of NADW at 53°N.

Conversely, years such as 1997 and 1999 show net obduction until the isopycnal bin at 27.3 kg m^{-3} and subduction for the densest isopycnal bins similar to what is observed in the thermodynamic approach. Another fundamental difference between the two approaches is the homogeneity of the horizontal distribution of the positive and negative formation rates within the isopycnal layers. The thermodynamic approach displays a more homogeneous distribution, with a clear separation between positive formation rate (subduction) primarily occurring in the southern part of the isopycnal layer and negative formation rate (obduction) happening in the northern part (see Figure 3). Consequently, when computing the net formation rate, the lightest densities, where negative formation rates occupy a larger area than positive formation rates, exhibit net obduction. On the other hand, the kinematic approach is less homogeneous due to large spatial variability driven by the horizonal currents. The entrainment component resembles the distribution observed in the thermodynamic approach and displays a more homogeneous pattern. Nevertheless, the time-series of net formation rate obtained only from the entrainment component still disagree with the time-series from the thermodynamic approach (see Figures 8b and 8c). This is most likely because the positive values of the formation rate are still higher than the negative values (see Figure 5).

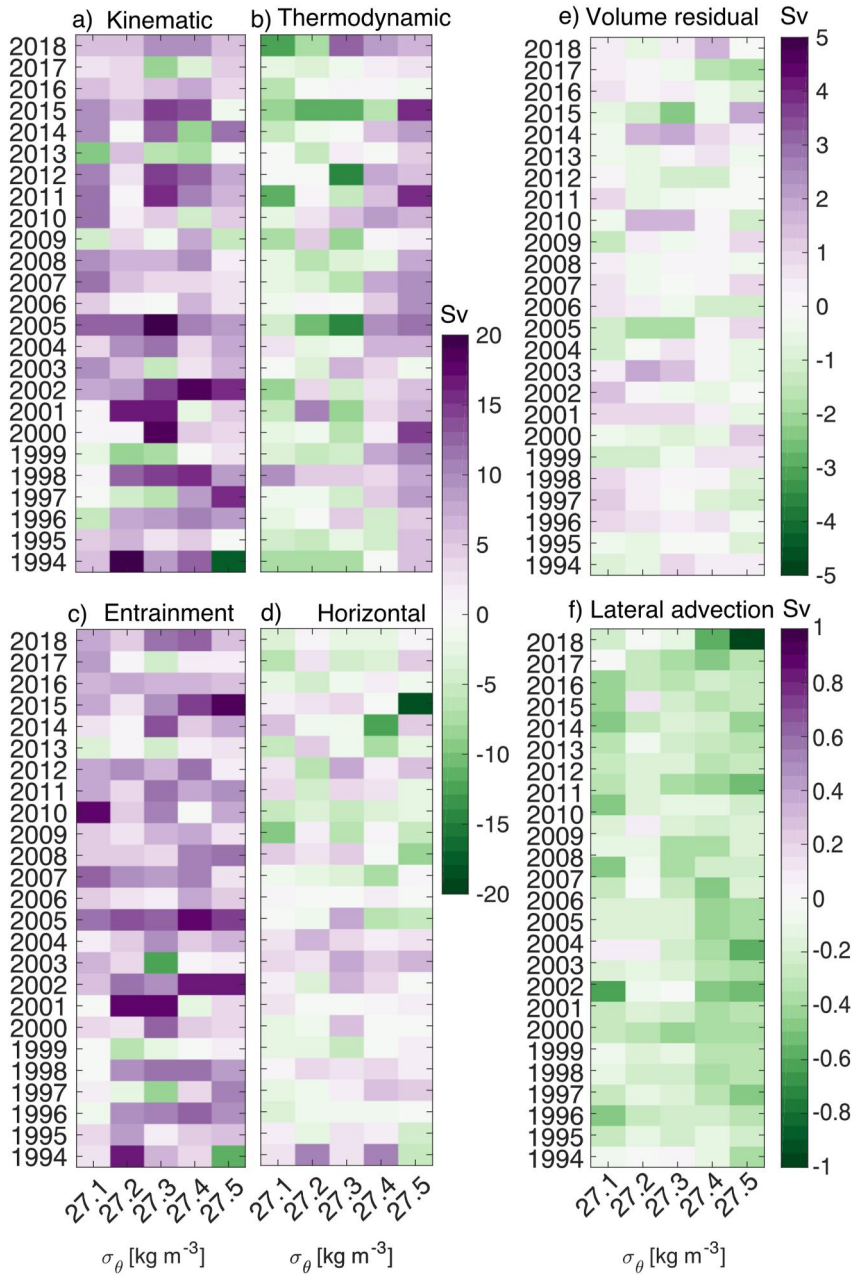

Figure 8. Hovmöller diagram of the formation rate in the isopycnal bins of the SPMW ranging from $\sigma_\theta = 27.1$ to 27.5 kg m^{-3} and calculated using the kinematic approach (a) with the corresponding components: entrainment (c) and horizontal (d), and using the thermodynamic approach (b). Volume residual expressed in [Sv] in (e) and lateral advection (outward negative) within the mixed layer [Sv] in (f). Note the different intervals and ranges of the color scales for the formation rates, the volume residual and lateral advection.

Furthermore, additional evidence in the support of the formation of SPMW by diapycnal mixing is presented by examining the lateral volume fluxes (lateral advection) within the mixed layers across the open boundaries (Figure 8f). The analysis of the volume residual (Figure 8e), calculated as the difference between the volume of SPMW formed in one specific year and the volume formed the previous year ($V_{(year)} - V_{(year-1)}$)/year, further strengthens this argument. This volume represents the accumulation or removal of SPMW over the year following its winter formation. The fact that the values of these fluxes (volume residuals and lateral advection) are lower than the formation of SPMW is an indication that most of the SPMW formed is transported away from the formation

region below the mixed layer. This is also the case if the values are compared with the values from the daily buoyancy fluxes (not shown).

3.2.1. Variability of the SPMW Formation Area

In this section, we discuss the variability of the horizontal distribution of formation rates from the two approaches. In the thermodynamic approach, we consistently observe positive formation rates (indicating subduction or production of a new water mass) in regions with the highest layer thickness, and negative formation rates (representing obduction or consumption of water masses) to the north of these high layer thickness regions (Figures 3f–3j). In the kinematic approach, the clear south/north separation between positive and negative formation rates is less prominent (Figures 3a–3i). There are significant deviations from the spatial mean distribution in Figure 3 from year to year, especially in the area where maximum formation occurs, as shown by the yearly mean spatial distribution for each isopycnal bin (refer to figures in Supporting Information S1). This substantial spatial variability poses a challenge in describing the temporal changes in SPMW formation rates solely based on fixed spatial observations such as moorings arrays and repeated hydrographic sections, as water production or consumption can occur at different locations each year.

With respect to the large interannual variability some years are more striking than others regarding either strong or weak formation followed by larger or smaller volume occupied by the SPMW. We analyzed those two situations by performing a composite analysis. In the composite 1 we grouped five years that shows the largest outcrop areas in the densest isopycnal layers—1995, 2000, 2009, 2015 and 2018—and calculated the spatial average of layer thickness and formation rate for the isopycnal bins at σ_θ = 27.1 kg m^{-3} (Figures 9a and 9g), 27.3 kg m^{-3} (Figures 9c and 9i), and 27.5 kg m^{-3} (Figures 9e and 9k) using the kinematic and thermodynamic approaches. In the composite 2 we grouped 5 years that shows the smallest outcrop area for the densest isopycnal bins—that is, 1998, 2004, 2010, 2023, and 2017—(Figures 9b, 9d, 9f, 9h, 9j, and 9l).

During periods with a large surface area of the isopycnal bin at σ_θ = 27.5 kg m^{-3} (Figures 9e and 9k), there is a correspondingly large formation area, leading to a substantial production of SPMW in this isopycnal bin and a high volume of SPMW. Both approaches show this pattern, although the kinematic approach exhibits more variability. In contrast, the lightest isopycnal bin (Figures 9a and 9g) exhibits the opposite behavior, with a smaller outcrop area, followed by smaller formation area and volume. In periods when the densest isopycnal at 27.5 kg m^{-3} occupies a small area (Figures 9f and 9l), we observe a smaller formation area followed by a reduced volume of SPMW in this isopycnal layer. The lightest isopycnal again displays the opposite behavior (Figures 9b and 9h). This suggests a compensation effect between the isopycnal layers. Large formation of SPMW in the lightest isopycnals corresponds to reduced volume in the densest isopycnals, and vice versa.

Changes in each isopycnal layer occur simultaneously, but signals propagate within the subpolar gyre along the gyre circulation with a certain delay. For instance, if the lightest isopycnals south of the Porcupine Bank have weak formation, this signal may propagate northward along the eastern boundary and reach the densest isopycnal with a delay of a few years, resulting in weak formation in these isopycnals. A recent study from Tooth et al. (2023) based on a model Lagrangian analysis supports this idea, showing a principal overturning pathway in the subpolar North Atlantic sourced from the central NAC branch along the subpolar front. Along this path water undergoes continuous densification by circulating horizontally across sloping isopycnals. The authors suggest a propagation signal of approximately 2 years for water to arrive in the Irminger Sea from the Iceland Basin, consistent with the findings of Bilò et al. (2022). Considering the significant interannual variability observed in the time series of the outcrop area, as well as the winter mixed layer depth, salinity, and temperature, the compensation effect revealed by the composite analysis is a result of the weak versus strong formation signal propagating from lighter to denser isopycnals. This variation occurs from year to year over the 26-year observation period.

4. Conclusions

In this study we examined the mean characteristics and the interannual variability of volume and formation rates of SPMW in the subpolar North Atlantic. We compared the formation rates computed with two different approaches, based on a kinematic and a thermodynamic formulation, respectively. We looked at the mean state of each SPMW density bin and investigated the interannual variability over the period 1993–2018. These complementary approaches have never been applied to observational data in the North Atlantic before.

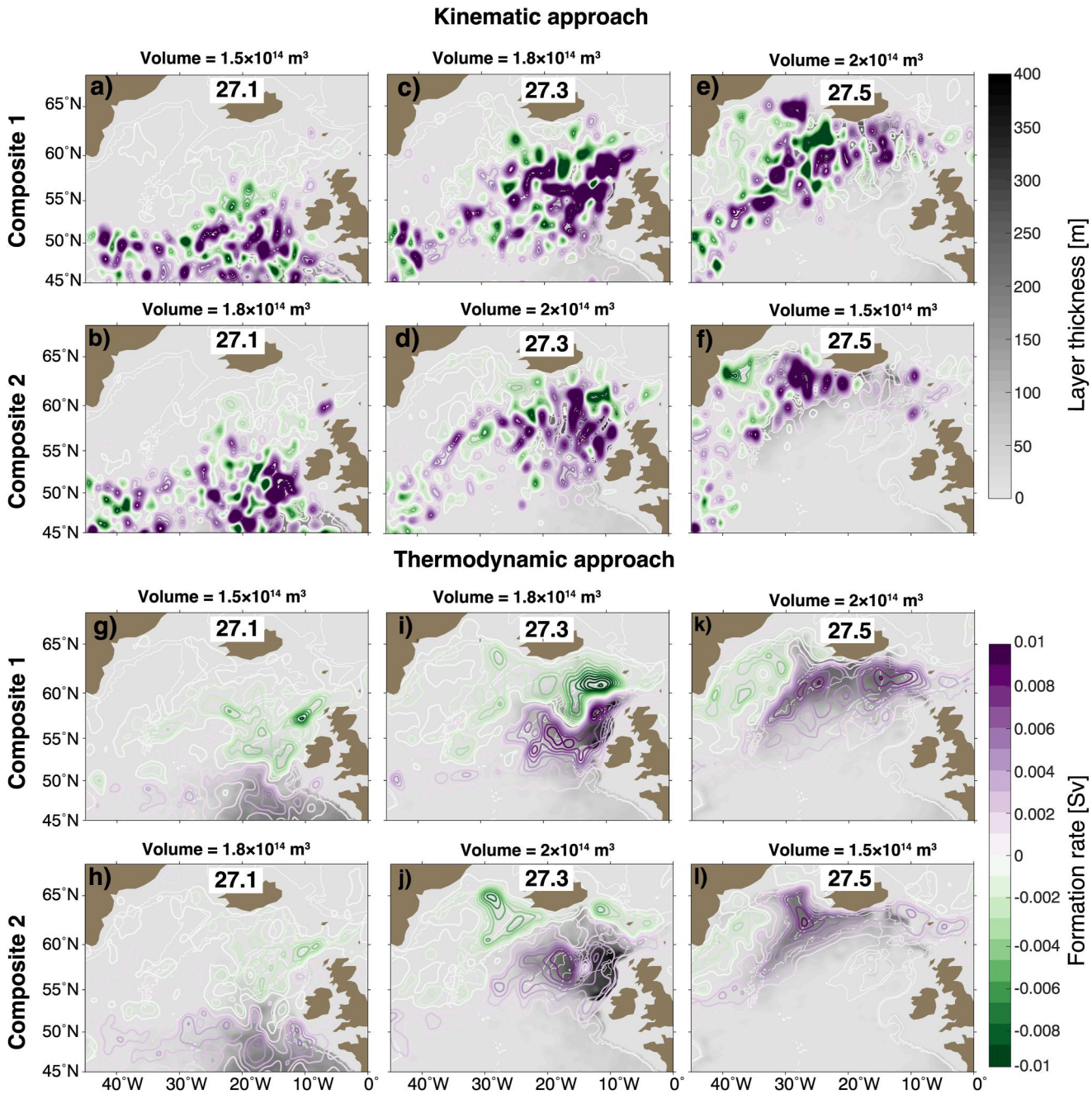

Figure 9. Composite maps of the SPMW layer thickness [m] (filled contour with gray color scheme). The color bar is displayed on the top right side, and formation rates [Sv] from the kinematic approach (a) to (f) and thermodynamic approach (g) to (l) for the isopycnal bins at $\sigma_0 = 27.1$ kg m^{-3} (first column a, b, g, and h), 27.3 kg m^{-3} (second column c, d, i, and j), and 27.5 kg m^{-3} (third column e, f, k, and l). The formation rate is depicted with contour lines using a purple/green color scheme. The purple contour lines are positive values and green contour lines are negative values (color bar on the bottom right side). The composite 1 (first row a, c, and e and third row g, i, and k) is calculated as the mean of the years 1995, 2000, 2009, 2015 and 2018. The composite 2 (second row b, d and f and fourth row h, j, and l) is calculated as the mean of the years 1998, 2004, 2010, 2013, and 2017. Bathymetry at 1,000 and 2,000 m is also displayed with gray contour lines. The mean volume of SPMW for each isopycnal bin is given on top of each panel.

About the mean state of SPMW, we observed that its spatial distribution within each isopycnal layer aligns well with the corresponding formation rate. However, the formation rate derived from the kinematic approach is much noisier than the thermodynamic one. This can be ascribed to the limits in the characterization of mesoscale and sub-mesoscale velocity components at the spatial and temporal resolution considered.

Our study contradicts the hypothesis proposed by Brambilla et al. (2008) regarding the transformation of SPMW. While they argue that SPMW transformation occurs separately within each NAC branch, our observations confirm the classical scheme proposed by McCartney and Talley (1982), pointing to a continuous transformation of SPMW from one density bin to the next denser one. Finally, the thermodynamic estimates indicate that air-sea interactions contribute to an increasing transformation rate of water masses between σ_θ = 26 kg m^{-3} and 27.3 kg m^{-3}, with the core formation occurring only between σ_θ = 27.4 kg m^{-3} and 27.5 kg m^{-3}. These findings align with previous studies by Grist et al. (2016) and Brambilla et al. (2008), also based on a thermodynamic approach. On the other hand, transformation rates obtained through the kinematic approach indicate net formation starting already at σ_θ = 27 kg m^{-3}. This apparent discrepancy suggests a significant influence of diapycnal mixing in diluting denser waters formed by air-sea fluxes, as discussed by Marshall et al. (1999).

Studies on SAMW in the Southern Ocean, such as Portela et al. (2020), have demonstrated the substantial impact of subduction and diapycnal mixing in shaping its volume changes. Considering the similarities in formation mechanisms between SAMW and SPMW, we can expect that enhanced diapycnal mixing near the MLD also plays a role in SPMW formation in the North Atlantic. A recent Lagrangian modeling study by Fröhle et al. (2022) also supports this hypothesis. In fact, the impact of diapycnal mixing emerges as the most plausible explanation for the differences observed here between the two methods, also because lateral fluxes across the open boundaries of our domain are negligible.

Water mass formation is mostly driven by mixed layer entrainment/detrainment. In fact, a swift shoaling of the mixed layer allows water to escape toward the ocean's interior, while a rapid destratification can allow previously subducted water to re-enter it. For mode waters, this mechanism described by Kwon et al. (2013) for the Southern Ocean and by Brambilla et al. (2008) for the North Atlantic, suggests detrainment mostly to occur in early spring, over an expanded outcrop area. Not having found SPMW below the winter mixed layer, Brambilla et al. (2008) excluded the classical advection down along the isopycnals as a significant contributor to SPMW formation. Our analysis confirms that entrainment/detrainment is the main driver of net subduction/obduction rates, but also acknowledges the role of lateral advection. We also find SPMW below the winter mixed layer, although its volume is smaller than during the summer period. This suggests a more complex dynamics than generally believed that drives the formation and subduction of SPMW.

Regarding the temporal variability of SPMW, we found that formation of SPMW is characterized by a large interannual variability, in both the amount and location of SPMW formed each year. During the 26 years analyzed, whenever the SPMW deepens and PV increases, the MLD becomes shallower, and vice versa. This relationship indicates that changes in PV and MLD are closely linked, as expected. The variability in PV and MLD corresponds also with changes of the outcrop area. When isopycnals shoal the outcrop area expands and when the isopycnals deepen the outcrop area contracts. Deeper mixed layers within wider outcrop areas tend to exhibit higher salinity and temperature, contrary to the expectation of colder and fresher water in deeper mixed layers. This may be explained by a stronger entrainment of deeper waters during these events. However, exceptions are also observed, particularly in cases where mixed layer deepening is associated with a small outcrop area, resulting in lower salinity and temperature like, for example, in 2002. Some years particularly stood out such as 1994–1995 and 2015. In those years, particularly large outcrop areas were followed by a deepening of the winter MLD, in the densest isopycnal bins. These years were also characterized by large SPMW formation rates and volumes. Conversely, in 1998 and 2013, small outcrop area led to weaker formation and small volumes in the denser isopycnal layers. For the lightest density bins, the same periods showed an opposite behavior. The formation of SPMW in the lightest isopycnals was compensated by reduced volumes in the densest isopycnal bins, and vice versa.

Our results support the idea that anomalies propagate within the subpolar gyre at interannual scales (see Bilò et al., 2022; Tooth et al., 2023). Formation in the lightest isopycnal bins potentially influences the formation in denser isopycnals with a delay of a few years. For example, the strong 2015 signal in the densest isopycnal bin could be the results of the large formation that took place well before, in 2013, in the lightest isopycnal layers. This lighter SPMW gradually propagated northward reaching the densest layers only in 2015. This significant interannual variability highlights the dynamic nature of water mass transformation processes, emphasizing the need for continued monitoring of the subpolar North Atlantic's oceanographic features.

Recent studies (Jackson & Petit, 2023; Petit et al., 2021) argued that surface fluxes are the main mechanisms responsible for the formation of water in the eastern North Atlantic. While mixing is able to modify densities and

shift the overturning profiles, it is still not significant in determining the strength of the overturning (Jackson & Petit, 2023). On the other hand, Fröhle et al. (2022) found that NADW crossing the latitude at 53°N is associated with a diapycnal mass flux, which accounts for up to 48% of the total flux. Other studies showed that changes observed in the last decades are caused by a reduced inflow of subtropical water masses (Biló et al., 2022) and by a larger contribution of surface water from the Labrador Sea (Fox et al., 2022). We also observed changes in the properties of the formed water masses, but their effect on the formation rates remains unclear. We do observe a large contribution of the surface fluxes in determining the formation of SPMW, but we also find that mixing plays an important role in distributing water across the isopycnals. This was clearly revealed by the mismatch between the kinematic and thermodynamic estimates. Further investigation and new approaches are thus necessary to determine whether the observed changes are the result of local modification in the air-sea fluxes or whether they originate from the propagation of anomalous signals from one region to the other, or both mechanisms are active. By using more advanced Lagrangian approaches, it should be in principle possible to understand how much of the SPMW that forms during winter is advected away from the region of formation and really contributes to the formation of cold limb of the AMOC and not re-entering the mixed layer in the following winter.

Data Availability Statement

This study has been conducted using E.U. Copernicus Marine Service Information: ARMOR3D (ARMOR3D, 2021, https://doi.org/10.48670/moi-00052), product ID: "Multi Observation Global Ocean 3D Temperature Salinity Height Geostrophic Current and MLD" (MULTIOBS_GLO_PHY_TSUV_3D_MY NRT_015_012) downloaded on the 7 January 2021, and OMEGA3D (Buongiorno Nardelli, 2020b, https://doi.org/10.25423/cmcc/multiobs_glo_phy_w_rep_015_007), product ID "Global Observed Ocean Physics 3D Quasi-Geostrophic Currents (MULTIOBS_GLO_PHY_W_3D_REP_015_007)." ERA5 reanalysis (Hersbach et al., 2023, https://doi.org/10.24381/cds.adbb2d47) is distributed by the Copernicus Climate Change Service (C3S) and downloaded on the 9 December 2021.

Acknowledgments
I.S. was supported by the Deutsche Forschungsgemeinschaft (DFG, Grant 440908407) as part of the project "Long-term ventilation changes of Subpolar Mode Waters in the North Atlantic Ocean and its impact on the oxygen distribution". D.I. and B.B.N. were supported by the EU H2020 project AtlantECO (Grant 862923). We thank the two anonymous reviewers who provided insightful and careful comments. Open Access funding enabled and organized by Projekt DEAL.

References

ARMOR3D. (2021). E.U. Copernicus marine service information (CMEMS) [Dataset]. Marine data store (MDS). Product ID: "multi observation global ocean 3D temperature salinity height geostrophic current and MLD (MULTIOBS_GLO_PHY_TSUV_3D_MYNRT_015_012). *ARMOR3D*. https://doi.org/10.48670/moi-00052

Berx, B., & Payne, M. R. (2017). The sub-polar gyre index - A community data set for application in fisheries and environment research. *Earth System Science Data*, *9*(1), 259–266. https://doi.org/10.5194/essd-9-259-2017

Biló, T. C., Straneo, F., Holte, J., & Le Bras, I. A. A. (2022). Arrival of new great salinity anomaly weakens convection in the Irminger Sea. *Geophysical Research Letters*, *49*(11), e2022GL098857. https://doi.org/10.1029/2022GL098857

Brambilla, E., & Talley, L. D. (2008). Subpolar mode water in the northeastern Atlantic: 1. Averaged properties and mean circulation. *Journal of Geophysical Research*, *113*(4), 1–18. https://doi.org/10.1029/2006JC004062

Brambilla, E., Talley, L. D., & Robbins, P. E. (2008). Subpolar mode water in the northeastern Atlantic: 2. Origin and transformation. *Journal of Geophysical Research*, *113*(C4), 4026. https://doi.org/10.1029/2006JC004063

Buckley, M. W., & Marshall, J. (2016). Observations, inferences, and mechanisms of the Atlantic meridional overturning circulation: A review. *Reviews of Geophysics*, *54*(1), 5–63. https://doi.org/10.1002/2015RG000493

Buongiorno Nardelli, B. (2020a). A multi-year time series of observation-based 3D horizontal and vertical quasi-geostrophic global ocean currents. *Earth System Science Data*, *12*(3), 1711–1723. https://doi.org/10.5194/ESSD-12-1711-2020

Buongiorno Nardelli, B. (2020b). CNR global observation-based OMEGA3D quasi-geostrophic vertical and horizontal ocean currents (1993-2018) (Version 1) [Dataset]. *Copernicus Monitoring Environment Marine Service (CMEMS)*. https://doi.org/10.25423/CMCC/MULTIOBS_GLO_PHY_W_REP_015_007

Buongiorno Nardelli, B., Guinehut, S., Verbrugge, N., Cotroneo, Y., Zambianchi, E., & Iudicone, D. (2017). Southern Ocean mixed-layer seasonal and interannual variations from combined satellite and in situ data. *Journal of Geophysical Research: Oceans*, *122*(12), 10042–-10060. https://doi.org/10.1002/2017JC013314

Buongiorno Nardelli, B., Mulet, S., & Iudicone, D. (2018). Three-dimensional ageostrophic motion and water mass subduction in the Southern Ocean. *Journal of Geophysical Research: Oceans*, *123*(2), 1533–1562. https://doi.org/10.1002/2017JC013316

Cerovečki, I., Talley, L. D., Mazloff, M. R., & Maze, G. (2013). Subantarctic mode water formation, destruction, and export in the eddy-permitting southern ocean state estimate. *Journal of Physical Oceanography*, *43*(7), 1485–1511. https://doi.org/10.1175/JPO-D-12-0121.1

Courtois, P., Garcia-Quintana, Y., Hu, X., & Myers, P. G. (2020). Kinematic subduction rate of labrador sea water from an eddy-permitting numerical model. *Journal of Geophysical Research: Oceans*, *125*(7), 1–21. https://doi.org/10.1029/2019JC015475

Da Costa, M. V., Mercier, H., & Treguier, A. M. (2005). Effects of the mixed layer time variability on kinematic subduction rate diagnostics. *Journal of Physical Oceanography*, *35*(4), 427–443. https://doi.org/10.1175/JPO2693.1

de Boisséson, E., Thierry, V., Mercier, H., Caniaux, G., & Desbruyères, D. (2012). Origin, formation and variability of the subpolar mode water located over the Reykjanes Ridge. *Journal of Geophysical Research*, *117*(C12), C12005. https://doi.org/10.1029/2011JC007519

de Boyer Montégut, C., Madec, G., Fischer, A. S., Lazar, A., & Iudicone, D. (2004). Mixed layer depth over the global ocean: An examination of profile data and a profile-based climatology. *Journal of Geophysical Research*, *109*(12), 1–20. https://doi.org/10.1029/2004JC002378

Dee, D. P., Uppala, S. M., Simmons, A. J., Berrisford, P., Poli, P., Kobayashi, S., et al. (2011). The ERA-interim reanalysis: Configuration and performance of the data assimilation system. *Quarterly Journal of the Royal Meteorological Society*, *137*(656), 553–597. https://doi.org/10.1002/QJ.828

Desbruyères, D. G., Chafik, L., & Maze, G. (2021). A shift in the ocean circulation has warmed the subpolar North Atlantic Ocean since 2016. *Commun Earth Environ*, *2*(1), 48. https://doi.org/10.1038/s43247-021-00120-y

Desbruyères, D. G., Mercier, H., Maze, G., & Daniault, N. (2019). Surface predictor of overturning circulation and heat content change in the subpolar North Atlantic. *Ocean Science*, *15*(3), 809–817. https://doi.org/10.5194/os-15-809-2019

Fox, A. D., Handmann, P., Schmidt, C., Fraser, N., Rühs, S., Sanchez-Franks, A., et al. (2022). Exceptional freshening and cooling in the eastern subpolar North Atlantic caused by reduced Labrador Sea surface heat loss. *Ocean Science*, *18*(5), 1507–1533. https://doi.org/10.5194/os-18-1507-2022

Fratantoni, P. S., & McCartney, M. S. (2010). Freshwater export from the Labrador Current to the North Atlantic Current at the tail of the grand banks of Newfoundland. *Deep-Sea Research Part I Oceanographic Research Papers*, *57*(2), 258–283. https://doi.org/10.1016/j.dsr.2009.11.006

Fröhle, J., Handmann, P. V. K., & Biastoch, A. (2022). Major sources of North Atlantic deep water in the subpolar North Atlantic from Lagrangian analyses in an eddy-rich ocean model. *Ocean Science*, *18*(5), 1431–1450. https://doi.org/10.5194/os-18-1431-2022

Giordani, H., Prieur, L., & Caniaux, G. (2006). Advanced insights into sources of vertical velocity in the ocean. *Ocean Dynamics*, *56*(5), 513–524. https://doi.org/10.1007/S10236-005-0050-1

Grist, J. P., Josey, S. A., Jacobs, Z. L., Marsh, R., Sinha, B., & Van Sebille, E. (2016). Extreme air–sea interaction over the North Atlantic subpolar gyre during the winter of 2013–2014 and its sub-surface legacy. *Climate Dynamics*, *46*(11–12), 4027–4045. https://doi.org/10.1007/s00382-015-2819-3

Groeskamp, S., Griffies, S. M., Iudicone, D., Marsh, R., Nurser, A. J. G., & Zika, J. D. (2019). The water mass transformation framework for ocean physics and biogeochemistry. *Annual Review of Marine Science. Annual Reviews*, *11*(1), 271–305. https://doi.org/10.1146/annurev-marine-010318-095421

Guinehut, S., Dhomps, A. L., Larnicol, G., & Le Traon, P. Y. (2012). High resolution 3-D temperature and salinity fields derived from in situ and satellite observations. *Ocean Science*, *8*(5), 845–857. https://doi.org/10.5194/os-8-845-2012

Hersbach, H., Bell, B., Berrisford, P., Biavati, G., Horányi, A., Muñoz Sabater, J., et al. (2023). ERA5 hourly data on single levels from 1940 to present [Dataset]. *Copernicus Climate Change Service (C3S) Climate Data Store (CDS)*. https://doi.org/10.24381/cds.adbb2d47

Holliday, N. P., Bersch, M., Berx, B., Chafik, L., Cunningham, S., Florindo-López, C., et al. (2020). Ocean circulation causes the largest freshening event for 120 years in eastern subpolar North Atlantic. *Nature Communications*, *11*(1), 585. https://doi.org/10.1038/s41467-020-14474-y

Iudicone, D., Madec, G., & McDougall, T. J. (2008). Water-mass transformations in a neutral density framework and the key role of light penetration. *Journal of Physical Oceanography*, *38*(7), 1357–1376. https://doi.org/10.1175/2007JPO3464.1

Iudicone, D., Madec, G., Blanke, B., & Speich, S. (2008). The role of Southern Ocean surface forcings and mixing in the global conveyor. *Journal of Physical Oceanography*, *38*(7), 1377–1400. https://doi.org/10.1175/2008JPO3519.1

Iudicone, D., Rodgers, K. B., Stendardo, I., Aumont, O., Madec, G., Bopp, L., et al. (2011). Water masses as a unifying framework for understanding the Southern Ocean Carbon Cycle. *Biogeosciences*, *8*(5), 1031–1052. https://doi.org/10.5194/bg-8-1031-2011

Jackson, L. C., Biastoch, A., Buckley, M. W., Desbruyères, D. G., Frajka-Williams, E., Moat, B., & Robson, J. (2022). The evolution of the North Atlantic meridional overturning circulation since 1980. *Nature Reviews Earth & Environment*, *3*(4), 241–254. https://doi.org/10.1038/s43017-022-00263-2

Jackson, L. C., & Petit, T. (2023). North Atlantic overturning and water mass transformation in CMIP6 models. *Climate Dynamics*, *60*(9–10), 2871–2891. https://doi.org/10.1007/s00382-022-06448-1

Karstensen, J., & Quadfasel, D. (2002). Formation of Southern Hemisphere thermocline waters: Water mass conversion and subduction. *Journal of Physical Oceanography*, *32*(11), 3020–3038. https://doi.org/10.1175/1520-0485(2002)032<3020:FOSHTW>2.0.CO;2

Kieke, D., Rhein, M., Stramma, L., Smethie, W. M., Bullister, J. L., & LeBel, D. A. (2007). Changes in the pool of Labrador Sea Water in the subpolar North Atlantic. *Geophysical Research Letters*, *34*(6), 1–5. https://doi.org/10.1029/2006GL028959

Kwon, E. Y., Downes, S. M., Sarmiento, J. L., Farneti, R., & Deutsch, C. (2013). Role of the seasonal cycle in the subduction rates of upper-southern ocean waters. *Journal of Physical Oceanography*, *43*(6), 1096–1113. https://doi.org/10.1175/JPO-D-12-060.1

Le Bras, I. A. A., Straneo, F., Holte, J., de Jong, M. F., & Holliday, N. P. (2020). Rapid export of waters formed by convection near the Irminger Sea's western boundary. *Geophysical Research Letters*, *47*(3), e2019GL085989. https://doi.org/10.1029/2019GL085989

Li, Z., England, M. H., Groeskamp, S., Cerovečki, I., & Luo, Y. (2021). The origin and fate of subantarctic mode water in the Southern Ocean. *Journal of Physical Oceanography*, *51*(9), 2951–2972. https://doi.org/10.1175/jpo-d-20-0174.1

Marsh, R., Josey, S. A., Nurser, A. J. G., De Cuevas, B. A., & Coward, A. C. (2005). Water mass transformation in the North Atlantic over 1985-2002 simulated in an eddy-permitting model. *Ocean Science*, *1*(2), 127–144. https://doi.org/10.5194/os-1-127-2005

Marshall, D. (1997). Subduction of water masses in an eddying ocean. *Journal of Marine Research*, *55*(2), 201–222. https://doi.org/10.1357/0022240973224373

Marshall, J., Jamous, D., & Nilsson, J. (1999). Reconciling thermodynamic and dynamic methods of computation of water-mass transformation rates. *Deep-Sea Research Part I Oceanographic Research Papers*, *46*(4), 545–572. https://doi.org/10.1016/S0967-0637(98)00082-X

McCartney, M. S., & Talley, L. D. (1982). The subpolar mode water of the North Atlantic Ocean. *Journal of Physical Oceanography*, *12*(11), 1169–1188. https://doi.org/10.1175/1520-0485(1982)012<1169:tsmwot>2.0.co;2

Mulet, S., Rio, M. H., Mignot, A., Guinehut, S., & Morrow, R. (2012). A new estimate of the global 3D geostrophic ocean circulation based on satellite data and in-situ measurements. *Deep Sea Research Part II: Topical Studies in Oceanography*, *77*(80), 70–81. https://doi.org/10.1016/J.DSR2.2012.04.012

Nishikawa, S., Tsujino, H., Sakamoto, K., & Nakano, H. (2010). Effects of mesoscale eddies on subduction and distribution of subtropical mode water in an eddy-resolving OGCM of the Western North Pacific. *Journal of Physical Oceanography*, *40*(8), 1748–1765. https://doi.org/10.1175/2010JPO4261.1

Nishikawa, S., Tsujino, H., Sakamoto, K., & Nakano, H. (2013). Diagnosis of water mass transformation and formation rates in a high-resolution GCM of the North Pacific. *Journal of Geophysical Research: Oceans*, *118*(3), 1051–1069. https://doi.org/10.1029/2012JC008116

Petit, T., Lozier, M. S., Josey, S. A., & Cunningham, S. A. (2021). Role of air-sea fluxes and ocean surface density in the production of deep waters in the eastern subpolar gyre of the North Atlantic. *Ocean Science*, *17*(5), 1353–1365. https://doi.org/10.5194/OS-17-1353-2021

Portela, E., Kolodziejczyk, N., Maes, C., & Thierry, V. (2020). Interior water-mass variability in the Southern Hemisphere oceans during the last decade. *Journal of Physical Oceanography*, *50*(2), 361–381. https://doi.org/10.1175/JPO-D-19-0128.1

Qiu, B., & Huang, R. X. (1995). Ventilation of the North Atlantic and North Pacific: Subduction versus obduction. *Journal of Physical Oceanography*, *25*(10), 2344–2360. https://doi.org/10.1175/1520-0485(1995)025<2374:votnaa>2.0.co;2

Rintoul, S. R. (2018). The global influence of localized dynamics in the Southern Ocean. *Nature*, *558*(7709), 209–218. https://doi.org/10.1038/s41586-018-0182-3

Sloyan, B. M., Talley, L. D., Chereskin, T. K., Fine, R., & Holte, J. (2010). Antarctic intermediate water and subantarctic mode water formation in the Southeast Pacific: The role of turbulent mixing. *Journal of Physical Oceanography*, *40*(7), 1558–1574. https://doi.org/10.1175/2010JPO4114.1

Speer, K., & Tziperman, E. (1992). Rates of water mass formation in the North Atlantic Ocean. *Journal of Physical Oceanography*, *22*(1), 93–104. https://doi.org/10.1175/1520-0485(1992)022<0093:rowmfi>2.0.co;2

Stendardo, I., Kieke, D., Rhein, M., Gruber, N., & Steinfeldt, R. (2015). Interannual to decadal oxygen variability in the mid-depth water masses of the eastern North Atlantic. *Deep-Sea Research Part I Oceanographic Research Papers*, *95*, 85–98. https://doi.org/10.1016/j.dsr.2014.10.009

Stendardo, I., Rhein, M., & Steinfeldt, R. (2020). The North Atlantic Current and its volume and fresh-water transports in the subpolar North Atlantic, time period 1993 - 2016. *Journal of Geophysical Research: Oceans*, *125*(9), e2020JC016065. https://doi.org/10.1029/2020JC016065

Stommel, H. (1979). Determination of water mass properties of water pumped down from the Ekman layer to the geostrophic flow below (subtropical gyre/Ekman pumping/water mass origins). *PNAS*, *76*(7), 3051–3055. https://doi.org/10.1073/pnas.76.7.3051

Tooth, O. J., Johnson, H. L., & Wilson, C. (2023). Lagrangian overturning pathways in the Eastern Subpolar North Atlantic. *Journal of Climate*, *36*(3), 823–844. https://doi.org/10.1175/JCLI-D-21-0985.1

Trossman, D. S., Thompson, L., Mecking, S., & Warner, M. J. (2012). On the formation, ventilation, and erosion of mode waters in the North Atlantic and Southern Oceans. *Journal of Geophysical Research*, *117*(9), C09026. https://doi.org/10.1029/2012JC008090

Walin, G. (1982). On the relation between sea-surface heat flow and thermal circulation in the ocean. *Tellus*, *34*(2), 187–195. https://doi.org/10.1111/J.2153-3490.1982.TB01806.X

Xu, X., Rhines, P. B., & Chassignet, E. (2018). On mapping the diapycnal water mass transformation of the Upper North Atlantic Ocean. *Journal of Physical Oceanography*, *48*(10), 2233–2258. https://doi.org/10.1175/JPO-D-17-0223.1

Zhang, R., Sutton, R., Danabasoglu, G., Kwon, Y. O., Marsh, R., Yeager, S. G., et al. (2019). A review of the role of the Atlantic meridional overturning circulation in Atlantic multidecadal variability and associated climate impacts. *Reviews of Geophysics*, *57*(2), 316–375. https://doi.org/10.1029/2019RG000644